informatics inc

(12)

FC

(12)

SOVIET MATERIAL ON INTERNAL WAVE EFFECTS

No. 5, March, 1976

Sponsored by

Defense Advanced
Research Projects Agency

DARPA Order No. 3097

March 15, 1976

DARPA Order No. 3097
Program Code No. P610, P6D10, P6E20, P6G10
Name of Contractor:
Informatics Inc.
Effective Date of Contract:
September 1, 1975
Contract Expiration Date:
February 29, 1976
Amount of Contract: $138, 147

Contract No. MDA-903-76C-0099
Principal Investigator:
Stuart G. Hibben
Tel: (301) 770-3000
Program Manager:
Ruth Ness
Tel: (301) 770-3000
Short Title of Work:
"Internal Waves"

This research was supported by the Defense Advanced Research Projects Agency and was monitored by the Defense Supply Service - Washington, under Contract No. MDA-903-76C-0099. The views and conclusions contained in this document are those of the author and should not be interpreted as necessarily representing the official policies, either express or implied, of the Defense Advanced Research Projects Agency or the United States Government.

Informatics Inc
Information Systems Company
6000 Executive Boulevard
Rockville, Maryland 20852
(301) 770-3000

UNCLASSIFIED

SECURITY CLASSIFICATION OF THIS PAGE *(When Date Entered)*

REPORT DOCUMENTATION PAGE

READ INSTRUCTIONS BEFORE COMPLETING FORM

1. REPORT NUMBER

2. GOVT ACCESSION NO.

3. RECIPIENT'S CATALOG NUMBER

4. TITLE (and Subtitle)
Soviet Material on Internal Wave Effects, Number 5, March 1976

5. TYPE OF REPORT & PERIOD COVERED
Scientific... Interim

6. PERFORMING ORG. REPORT NUMBER

7. AUTHOR(s)
Stuart G. Hibben, John Kourilo, B. L. Shrestha and M. Ness

8. CONTRACT OR GRANT NUMBER(s)
MDA-903-76C-0099

9. PERFORMING ORGANIZATION NAME AND ADDRESS
Informatics, Inc.
6000 Executive Boulevard
Rockville, MD 20852

10. PROGRAM ELEMENT, PROJECT, TASK AREA & WORK UNIT NUMBERS
DARPA Order No. 3097
Program Code No. P6L10, P6D10, P6E20, P6G10

11. CONTROLLING OFFICE NAME AND ADDRESS
Defense Advanced Research Projects Agency/TAO
1400 Wilson Boulevard
Arlington, VA 22209

12. REPORT DATE
March 15, 1976

13. NUMBER OF PAGES
95

14. MONITORING AGENCY NAME & ADDRESS *(if different from Controlling Office)*
Defense Supply Service - Washington
Room 1D245, Pentagon
Washington, D.C. 20310

15. SECURITY CLASS. *(of this report)*
UNCLASSIFIED

15a. DECLASSIFICATION/DOWNGRADING SCHEDULE

16. DISTRIBUTION STATEMENT *(of this Report)*

Approved for public release; distribution unlimited

12 100p.

17. DISTRIBUTION STATEMENT *(of the abstract entered in Block 20, if different from Report)*

18. SUPPLEMENTARY NOTES

Scientific... Interim

19. KEY WORDS *(Continue on reverse side if necessary and identify by block number)*
Internal waves
Capillary waves
Surface signature
Turbulent flow
Ocean microstructure

20. ABSTRACT *(Continue on reverse side if necessary and identify by block number)*

This is the fifth collection of abstracts of recent Soviet articles on generation and detection of internal waves. It is based on items listed in the fifth Bibliography of Soviet Material on Internal Waves, published November 10, 1975, and covering material received from June through October 1975.

which covers June - Oct 1975.

The abstracts are divided into internal effects and surface effects, comprising active and passive measurement of wave states. An author index is appended.

DD FORM 1 JAN 73 1473 EDITION OF 1 NOV 65 IS OBSOLETE

UNCLASSIFIED 387 113

SECURITY CLASSIFICATION OF THIS PAGE *(When Date Entered)*

INTRODUCTION

This is the fifth collection of abstracts of recent Soviet articles on generation and detection of internal waves. It is based on items listed in the fifth Bibliography of Soviet Material on Internal Waves, published November 10, 1975, and covering material received from June through October 1975.

The abstracts are divided into internal effects and surface effects, comprising active and passive measurement of wave states. An author index is appended.

TABLE OF CONTENTS

1. Internal Effects

Arsen'yev, S. A., S. V. Dobroklonskiy, R. M. Mamedov, and N. K. Shelkovnikov. Direct measurements of characteristics of small-scale sea turbulence, taken from a stationary platform in the open ocean. FAiO, no. 8, 1975, 845-850.

Measurements of Reynolds stress and other turbulence parameters in the 0.005-5 Hz range were performed in the Caspian Sea, 27 km off of Artem Island, in the presence of surface waves. The water depth in the measurement area was 37 m, salinity 10‰. The measurements were supplemented with observations on hydrological conditions. The instrumentation (see Fig. 1) used a hot wire anemometer for flow velocity measurement, rated at a temperature-independent sensitivity of 2 V sec/cm at $\bar{U}$ = 10 cm/sec. Fluctuations in flow velocity components were measured with an error of 10%, while wind velocity, mean temperature, and mean flow velocity were measured with errors at $\pm$ 1 m/sec, $\pm$ 0.01° C, and $\pm$ 2 cm/sec, respectively. Observation and averaging periods for $\bar{u}^2$, $\bar{w}^2$ and $\rho\,\overline{uw}$ were 30 min.

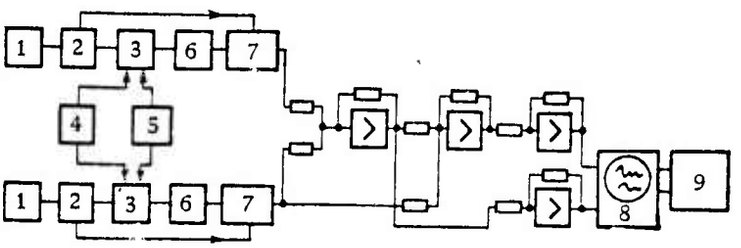

Fig. 1. Block-diagram of apparatus for measuring fluctuations of flow velocity components.

1- generator; 2- power amplifier; 3- transformer bridge; 4- velocity sensor; 5- temperature compensation sensor; 6- unbalance amplifier; 7- phase detector; 8- two-beam oscilloscope; 9- correlometer.

The results are shown in Figs. 2-4 and Tables 1 and 2.

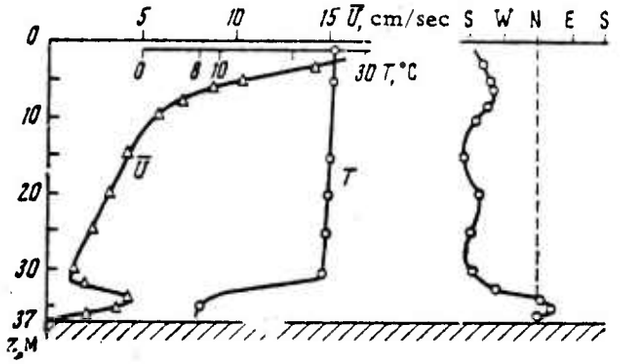

Fig. 2. Vertical profiles of mean velocity, mean temperature, and mean flow direction.

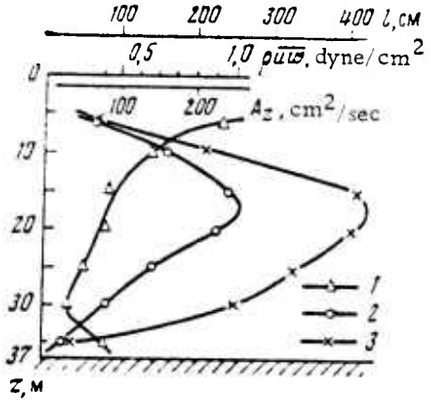

Fig. 3. Vertical profiles of the Reynolds stress (1), coefficient of eddy viscosity (2), and turbulence (3).

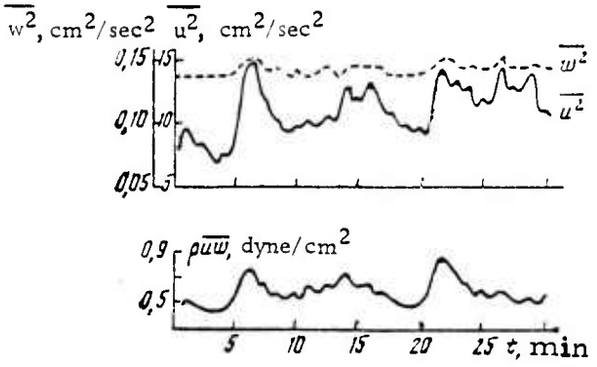

Fig. 4. Time variations of $\overline{u}^2$, $\overline{w}^2$, and $\rho\,\overline{uw}$.

Table 1

z	$\rho\overline{uw}$, dyne/см^2	A_z, см^2/sec	l, см	$(\overline{u^2})^{1/2}$, см/sec	$(\overline{w^2})^{1/2}$, см/sec	I_u	I_{10}	r	a
6	−0,95	63	65	5,1	0,45	0,51	0,045	−0,42	11
10	−0,57	163	216	3,3	0,38	0,55	0,063	−0,45	8,7
15	−0,34	243	416	2,8	0,30	0,56	0,060	−0,40	9,2
20	−0,32	228	404	2,4	0,28	0,60	0,070	−0,48	8,6
25	−0,20	143	327	2,5	0,21	0,83	0,070	−0,38	12
30	−0,13	80	257	5,3	0,19	2,60	0,095	−0,13	28
35	−0,32	20	34	3,8	0,26	0,76	0,052	−0,35	14

Table 2

Rate of dissipation of turbulent energy

z, m	ϵ, cm^2/sec^3	z, m	ϵ^*, cm^2/sec^3
6	1.4×10^{-2}	1	4.2×10^{-2}
10	2.0×10^{-3}	2	2.2×10^{-2}
15	4.8×10^{-4}	12	2.5×10^{-4}
20	4.5×10^{-4}	-	-
25	2.8×10^{-4}	-	-
30	1.8×10^{-4}	-	-
35	5.1×10^{-3}	-	-

* Results of Stewart and Grant (1962).

The cited results suggest that generation of turbulence by breaking of surface waves becomes significant only for appreciable wind velocities. The resulting enhanced values of Reynolds stress and coefficient of eddy viscosity are due to measurements in a shallow sea and over a wide range of frequencies.

Babiy, M. V., and L. V. Cherkesov. Generation of internal waves in the coastal zone. Morskiye gidrofizicheskiye issledovaniya, no. 2, 1974, 13-22.

The problem of generation of long internal waves in a two-layered sea with varying depth (see Fig. 1) by periodic surface waves which propagate towards a coast is solved by an analytical-numerical method. This article deals with reflection and transmission of internal waves which propagate from a deep to shallow water region as well.

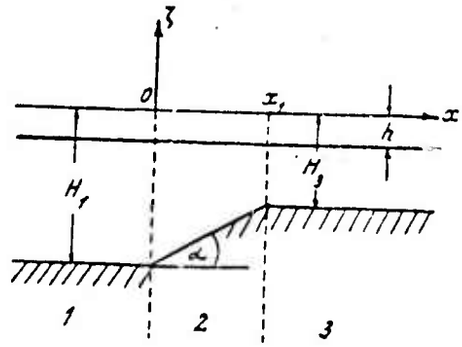

Fig. 1. Two-layer model.

The calculations show that surface waves, while propagating over a transition with a linearly varying depth, generate internal waves which propagate both towards deep and shallow-water regions. The amplitudes of the internal waves propagating in the opposite direction, $\overline{B}_2$ and $\overline{B}_3$, are approximately equal to each other and can readily exceed the amplitudes of the surface waves, A_1. The amplitudes $\overline{B}_2$ and $\overline{B}_3$ increase with an increase of h, α, and H_1-H_3; they decrease with an increase of the density discontinuity (ϵ); and are independent of α, the frequency of the internal waves (σ), and the Coriolis force (ω) for large angles of slope. Some analytical results for the amplitude of internal waves are shown in Figs. 2-4.

The distortion of internal waves which propagate from a deep to a shallow-water region is determined mainly by the thickness of the lower water layer in the shallow-water region. The dependence of the reflection and transmission coefficients, r_1 and r_2, upon $h_3 = H_3$-h and the frequency of the internal waves are shown in Figs. 5 and 6, respectively. Furthermore, the coefficient r_1 increases while r_2 decreases with an increase of α. However, these coefficients are independent of α, σ, and ω for large angles of slope.

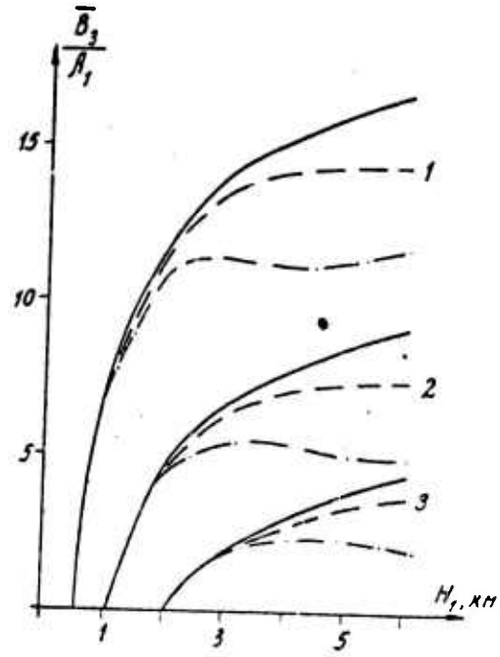

Fig. 2. Function $\bar{B}_3$ (H_1) for three H_3 values.

$\sigma = 1.4 \times 10^{-4}$ sec^{-1}; $\epsilon = 10^{-3}$; h = 200 m; $\omega = 0$; $\alpha = 89°30'$ (solid lines), 10° (dotted lines), 5° (dot-dashed lines). Curves 1-3 - H_3 = 0.5, 1, 2 km.

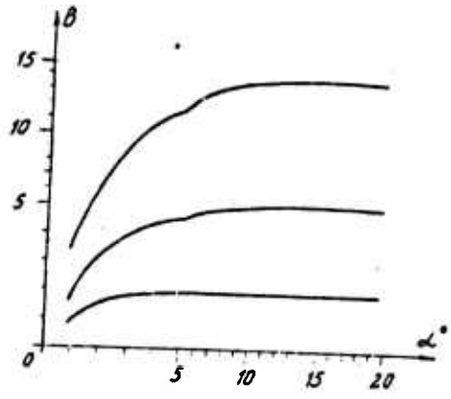

Fig. 3. Function $\bar{B}_3$ (α).

$\sigma = 1.4 \times 10^{-4}$ sec^{-1}; H_1 = 4 km; h = 500 m; $\epsilon = 10^{-3}$; H_3 = 1, 2, 3 km.

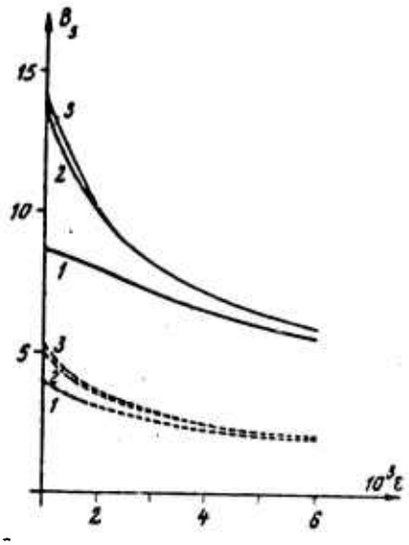

Fig. 4. Function $B_3(\epsilon)$ for three α values.

$\sigma = 1.4 \times 10^{-4}$ sec^{-1}; H_1 = 4 km; h = 500 m;
H_3 = 1 (solid lines), 2 km (dashed lines);
α = 3, 10, and 45° (curves 1, 2, and 3, resp).

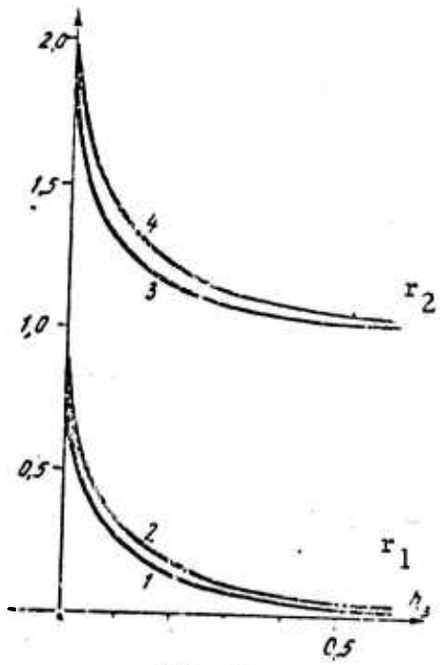

Fig. 5.

$\sigma = 10^{-4}$ sec^{-1}; $\epsilon = 10^{-3}$; $\alpha = 10^{\circ}$; 0.5 km $\leq H_3 \leq$ 1 km;
100 m $\leq h \leq$ 500 m.
Curves 1, 3 - H_1 = 1 km; Curves 2, 4 - H_1 = 6km.

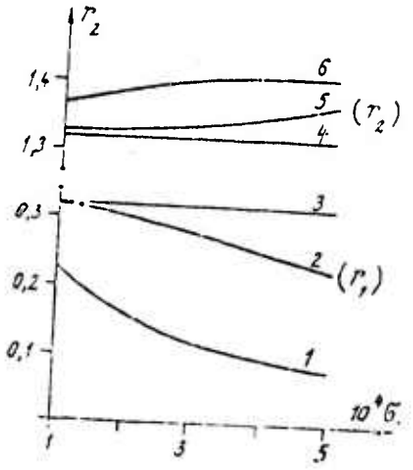

Fig. 6.

Curves 1, 6 - $\alpha = 2^\circ$; Curves 2, 5 - $\alpha = 10^\circ$;
Curves 3, 4 - $\alpha = 89^\circ 30'$.

Babiy, M. V. Generation of internal waves in a coastal zone (three-layered model). Morskiye gidrofizicheskiye issledovaniya, no. 2, 1974, 23-30.

In a companion article to the foregoing, the problem of generating long internal waves in a three-layered sea (see Fig. 1) by periodic surface waves is solved by an analytical-numerical method in the framework of linear wave theory.

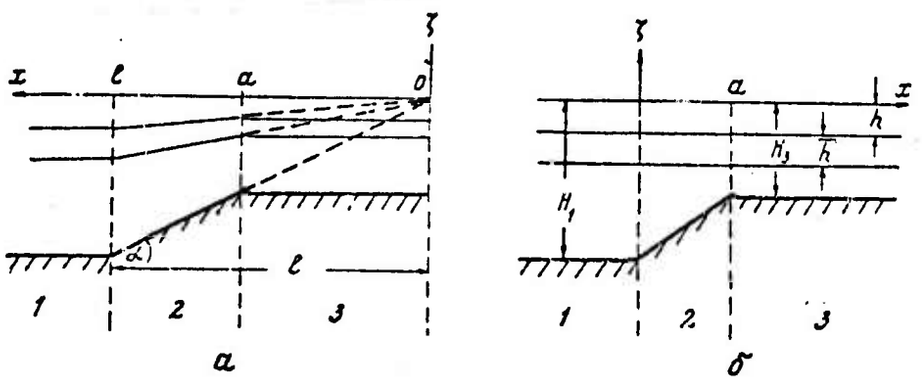

Fig. 1. Three layer model.

The study shows that surface waves propagating through a transition zone with a linear variation of the lowermost layer of a three-layered sea generate internal waves with two discrete wavelengths; their amplitudes exceed by a factor of two or greater the amplitudes of the surface waves. The relationship between the internal wave amplitudes at the upper ($\bar{B}$, $\bar{C}$) and lower ($\bar{\bar{B}}$, $\bar{\bar{C}}$) interfaces depends strongly on the corresponding density jumps ($\epsilon_1 = \rho_2 - \rho_1/\rho_2$; $\epsilon_2 = \rho_3 - \rho_2/\rho_3$). Also, the amplitudes of all internal waves thus generated increase with the thickness of the upper layers (h, $\bar{h}$). Similarly, the difference between the amplitudes of shorter internal waves in shallow- and deep-water regions (C_2, C_3) grows with increased h. The amplitudes of the internal waves depend on the slope of the bottom in the transition region only when $\alpha < 20^\circ$, when they increase with α.

However, if the thickness of the two upper layers in the transition zone varies proportionally to the change of the overall thickness (Fig. 1, a), internal waves are not generated.

Belyayev, V. S., I. D. Lozovatskiy, and R. V. Ozmidov. Parameters of small-scale turbulence and their connection with local stratification conditions in the ocean. FAiO, v. 11, no. 7, 1975, 718-725.

Simultaneous measurements of fluctuations of flow velocity u' and electrical conductivity σ' in the 1-150 Hz range, and temperature T were made during the 7-th cruise of the R/V Dmitriy Mendeleyev. The temperature was measured by a towed thermistor chain. The velocity and conductivity fluctuation sensors were mounted on a twin-casing towed body. Two 6m-spaced thermistors were located below the towed body, one thermistor was attached it, and two 1 m-spaced thermistors were located above the towed body (nos. 1-5, respectively).

The turbulence parameters calculated and the background hydrological conditions are given in the following table.

Table

Level	1	2	3	4	5	6	7	8	9	10	11	12
Depth, m	43	55	65	80	90	105	115	129	187	150	120	100
Towed body speed V, m/sec	2.7	3.0	3.1	3.2	3.2	3.2	3.2	3.3	1.7	1.9	1.9	1.9
s_u^2, cm^2/sec^2	260	140	7	4	2	4	3	4	0.4	0.2	0.2	0.2-1.0
s_σ^2, 10^{-4} ohm^{-2} cm^{-2}	4	4	4	4	4-15	4-30	6-40	10	25	9	4	4-60
$\Delta T/\Delta z$, deg/m	0	0	0.1	0.2	0.3	0.2	0.2	0.2	0	0.1	0.5	0.2-1.5
L, m	35	7	3	8	4	5	3	2	5	7	2	1
ΔU, cm/sec	19	5	6	8	2	9	5	2	-	4	1	1
Re x 10^{-4}	660	35	18	64	8	45	15	4	-	28	2	1

The results of measurements at level no. 12 in the table are of special interest. In contrast to the records at other levels of measurements, the time variation of the temperature T at level no. 12 is irregular, while ΔT between thermistors are variable, as shown in Fig. 1. As the figure

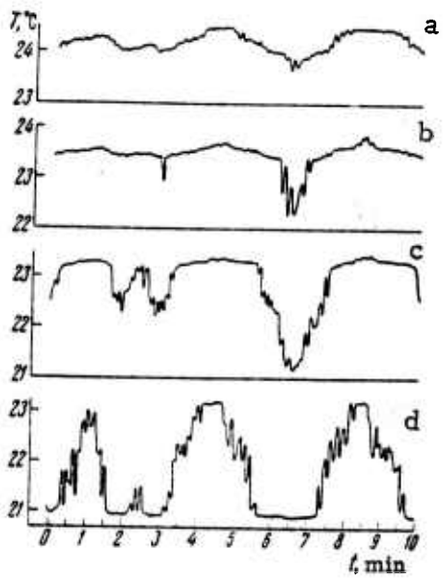

Fig. 1. Time variation of the temperature T at 100 m from data of thermistors no. 5(a), no. 4(b) no. 3(c), and no. 1(d).

indicates, the local temperature field has a fine structure: quasisothermic layers alternate with a gradient layer. The dependence of s_u^2/V (Ri) calculated for that level is the reciprocical of the hyperbolic one established for other levels as shown in Figure 2.

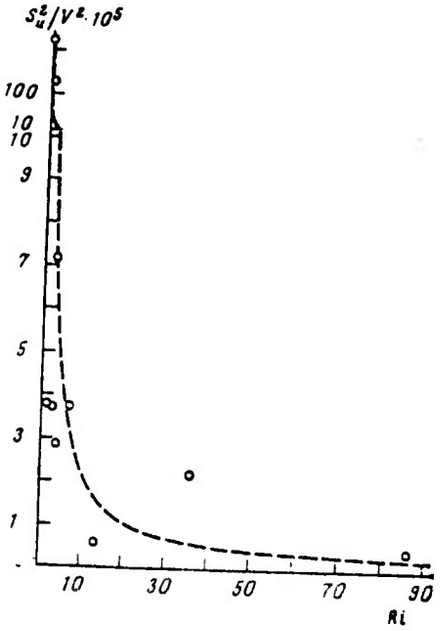

Fig. 2.

High levels of turbulence (portions 1, 3, 4 in Fig. 3) are attributed to breaking of internal waves.

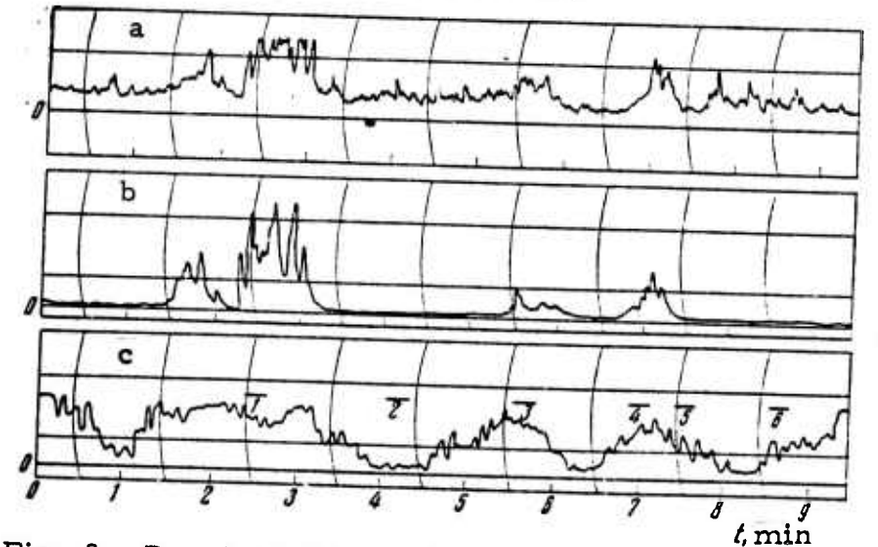

Fig. 3. Running variance for u'(a) and σ'(b) and time variation of Δ T at level no. 12.

This suggestion is supported by the nature of the dependence of the spectral density on $|\Delta(\Delta T/\Delta z)/\Delta x|$ (see Fig. 4). Further, the relationship of

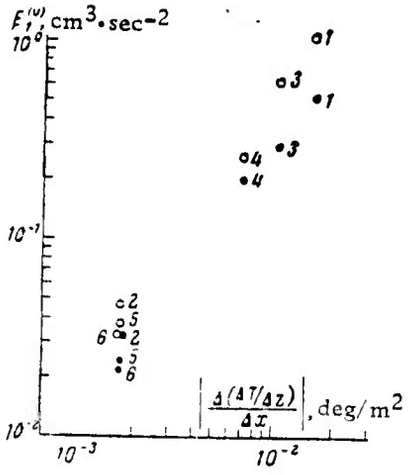

Fig. 4.
dots - k = 1 cm^{-1}; circles - k = 0.5 cm^{-1}.

turbulence to local conditions is indicated by small Re numbers ranging from 10^{-4} - 10^{-5}. Moreover, the experimental spectra for u' follow the universal spectrum of turbulence in the inertial-viscous interval for large Re, and deviate from it for Re = 2×10^{-3} - 4×10^{-4} (see Fig. 5). Thus, the hypothesis of small Re numbers for turbulence in a stratified ocean is experimentally verified.

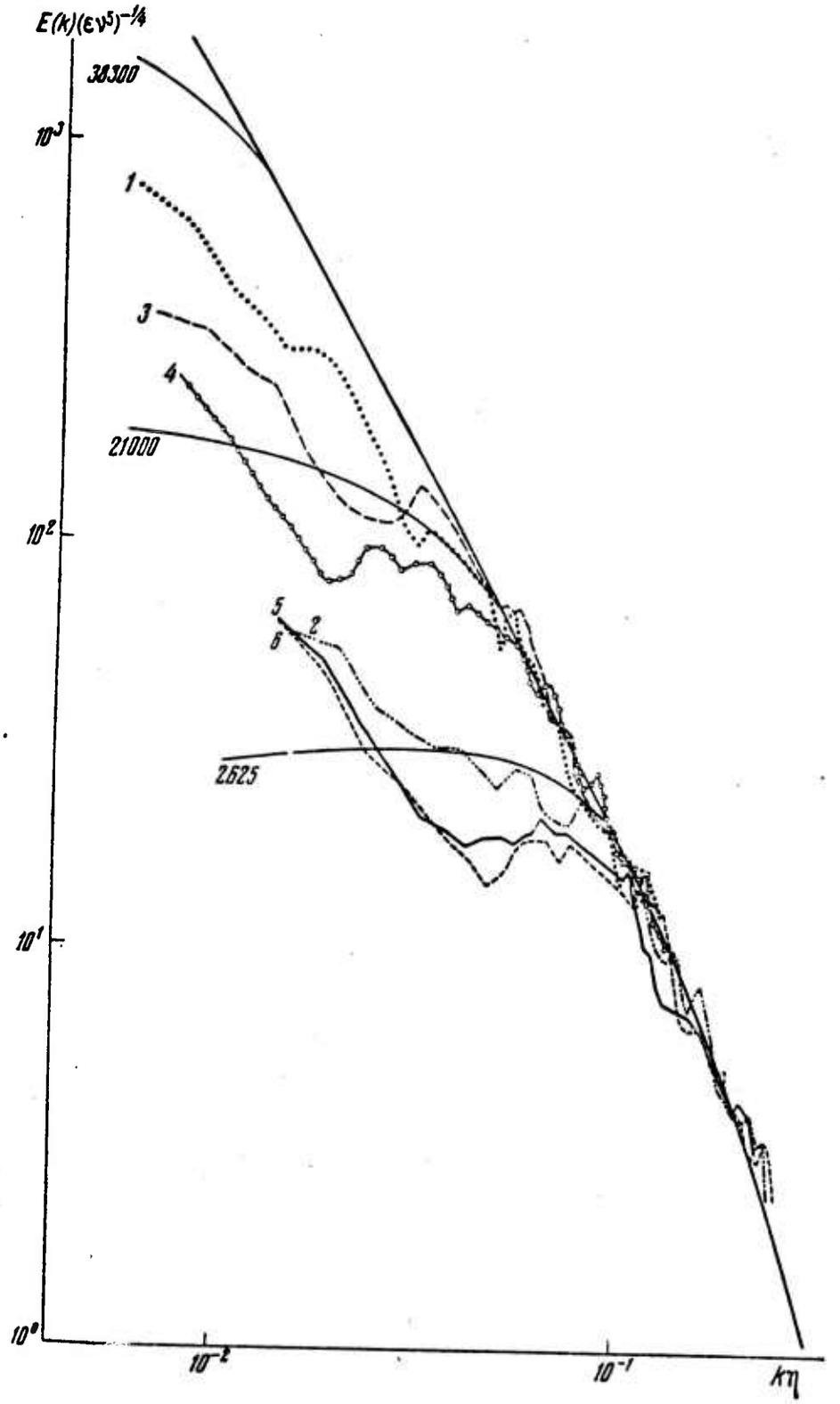

Fig. 5. Normalized spectral density for u' and turbulence spectra from laboratory measurements (solid lines).

Belyayev, V. S., R. V. Ozmidov, A. M. Trokhan, and S. R. Stefanov. Comparative measurements of small-scale fluctuations of hydrophysical fields in the ocean, using different types of instruments. Okeanologiya, no. 3, 1975, 534-537.

Comparative measurements during the 11th cruise of the R/V Dmitriy Mendeleyev in 1974 were made using hot-film meter, a "hydroresistor" type current meter, and optoacoustic sensor for simultaneous measurements of fluctuations of two horizontal components of flow velocity and sound speed (see Figs. 1 and 2).

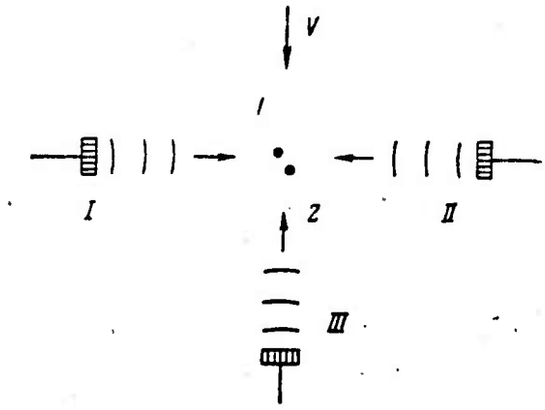

Fig. 1. Schematic diagram of the optoacoustical sensor.

I, II, III - ultrasound emitters. 1, 2 - light beams, perpendicular to the vectors of ultrasonic waves.

The sensitive element in the hot-film anemometer is a platinum film deposited on quartz glass in the form of two split rings. The thickness of the film is 0.0001 cm and its resistance is 4-6 ohms. The frequency range of the instrument is 1.5 - 150 Hz, while rms noise level is equivalent to a velocity of 0.12 mm sec^{-1}. The effect of temperature fluctuations is such that a temperature change of 1° C is equivalent to a velocity change of 20 cm sec^{-1} (for heating to 20° over ambient).

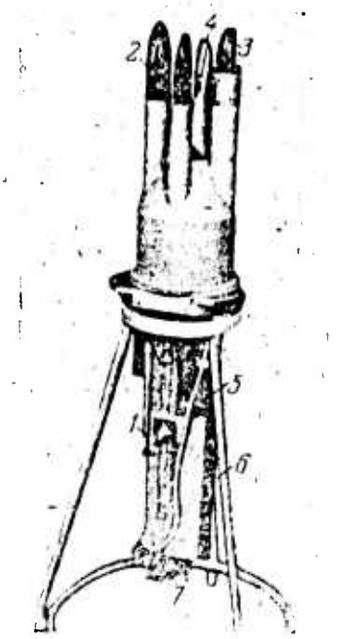

Fig. 2. General view of the optoacoustic instrument.

1 - OKG-13 gas laser; 2, 3 - optics;
4 - piezoceramic emitters; 5 - electronic unit;
6 - high-voltage unit; 7 - connectors

The sensing element in the "hydroresistor" current meter is a small volume of water between two electrodes, which is cooled by water flow. The frequency range of the instrument is 1-1000 Hz, while noise does not exceed 0.5 mmsec^{-1}.

The operating principle of the optoacoustical instrument is based on optical recording of the propagation velocity of ultrasound in a measurement area, isolated by two light (laser) beams. The maximum resolution of the instrument is 3 mm sec^{-1} for a signal-to-noise ratio equal to unity. The frequency range is 0.1-1000 Hz, and the measurement base is 5 mm (distance between laser beams).

Examples of spectral densities for fluctuations in flow and sound velocity as determined from observations made by the different instruments, are shown in Figs. 3 and 4.

Fig. 3. Spectral densities for fluctuations of flow velocity.

1-3 - longitudinal component from measurements by optical-acoustical instruments at depths of 5, 50, and 80 m;

4 and 5- the same, from measurements by "hydro-resistor" type current meter at depths of 34 and 74 m;

6- the same, from measurements by a hot-film current meter at a depth of 75 m;

7- transverse component from measurements by optical-acoustical instrument at a depth of 50 m.

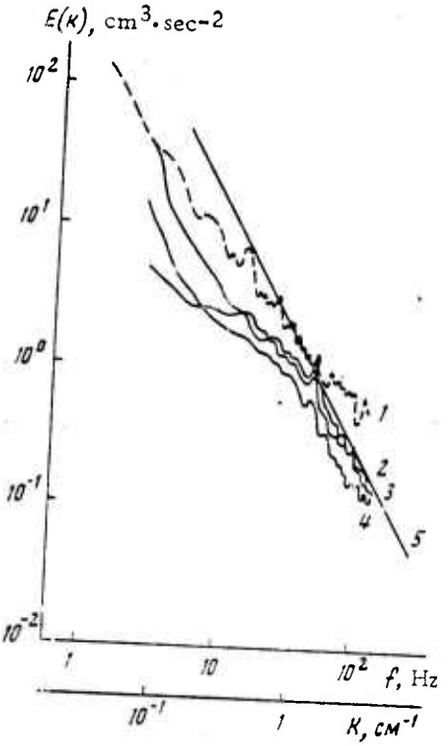

Fig. 4. Spectral densities for fluctuations of sound speed.

2-4 - from measurements by optoacoustic instrument at depths of 80, 50, and 15 m;

1- calculated from spectra for temperature fluctuations.

5 - "(-)5/3 power" law.

It is pointed out that the optoacoustic measurements demonstrated their working feasibility, but also their complexity and low reliability. In contrast to the other two instruments, they are hence not recommended for routine measurements.

Borisenko, Yu. D. Excitation of internal waves by a moving pressure system in a two-layer liquid. FAiO, no. 6, 1975, 660-664.

A model is considered in which a moving pressure $p = p_0 \cos(\Omega t - kx)$ is exerted on the surface of an ideal two-layer liquid. The thickness of the upper layer is h, while the lower layer extends without bound. Internal waves excited at the interface between the layers are analyzed without imposing requirements for infinitesimal wave amplitudes. A system of equations describing temporal changes in the amplitude and phase of the internal waves is obtained. This system of equations is qualitatively analyzed in the phase plane, and the growth of the internal waves is numerically estimated.

The solution of Laplace equations for velocity potentials in the upper and lower layers, which satisfies the boundary conditions at the free surface and the interface, is found by the Krylov-Bogolyubov asymptotic expansion method. The solution is found in the vicinity of the main resonance $|\omega - \Omega| \ll \epsilon^{1/2}\omega$ where ω is the frequency of the internal waves with infinitesimal amplitudes and ϵ is the nondimensional amplitude of the force exerted, $\epsilon = p_0 k/\rho_1 g$; in a real ocean $\epsilon \ll 1$. The solution is found in the form

$$\begin{aligned} dA/dt &= \varepsilon^{1/3}(\omega/2k)\, M(kh)\cos\theta, \\ \frac{d\theta}{dt} &= \omega - \Omega - \varepsilon^{1/3}(\omega/2kA)\, M(kh)\sin\theta + {}^1/_2\varepsilon^{2/3}\omega k^2 A^2 N(kh), \end{aligned} \tag{1}$$

where $M(kh) = e^{-kh}$ and $N(kh) = [3 - 8\,\mathrm{th}\,kh + 6\,\mathrm{th}^2 kh - 5\,\mathrm{th}^3 kh]/4\,\mathrm{th}^3 kh$.

The stationary solution of Eq. (1) is shown in Fig. 1. Steady internal waves, which change strictly periodically with time, correspond to stationary values of amplitude and phase. At exact resonance, $\Omega = \omega$, the stationary amplitude is finite and is given by $A = (M/N)^{1/3}/k$, $\theta = \pi/2$. At $\Omega < \omega\,(1 + 3\epsilon^{2/3} 2^{-5/3} M^{2/3} N^{1/3})$ there exists one stationary solution (curve I, Fig. 1). The corresponding phase trajectory pattern is shown in Fig. 2, a. The phase for these trajectories within the trajectory passing (0, 0)

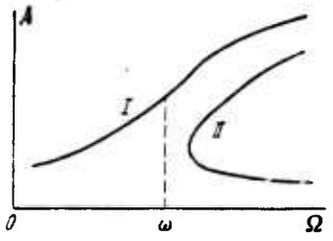

Fig. 1. Resonance curve in the vicinity of the main resonance $|\omega - \Omega| \leq \epsilon^{1/2} \omega$.

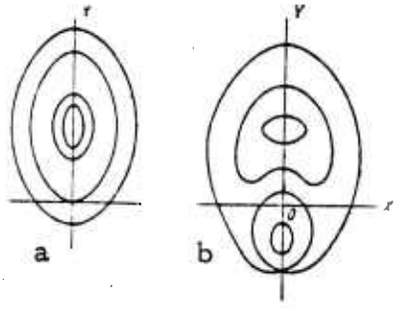

Fig. 2. Phase trajectory patterns.

changes periodically, while phase for outside trajectories changes monotonically. At $\Omega > \omega\ (1 + 3\epsilon^{2/3} 2^{-5/3} M^{2/3} N^{1/3})$ there exist three stationary solutions. The corresponding phase trajectory pattern is shown in Fig. 2, b. The lower portion of curve II in Fig. 1 in the phase plane defines the center, the upper portion - the saddle point. All phase trajectories are closed, hence the amplitude A is a bounded function of time, changing periodically, under any initial conditions. The phase θ can change either periodically or monotonically, depending on initial conditions.

The time T_{max} in which the amplitude of internal waves reaches a maximum, together with other parameters calculated for p_o = 5 mbar, h = 100 m, and $\beta = 10^{-3}$ (β is a parameter in the dispersion equation) are given in the table below.

	λ = 300 m	λ = 500 m	λ = 10 km
ω, sec^{-1}	1.01×10^{-2}	7.50×10^{-3}	5.90×10^{-4}
T	10 min	14 min	3 hour
ϵ	1.06×10^{-3}	6.42×10^{-4}	3.20×10^{-5}
kh	2.09	1.26	0.06
M	0.124	0.284	0.942
N	1.49	1.47	2.94×10^{3}
A_{max}, m	33	73	-
A_{st}, m	21	46	-
T_{max}	33 hour	36 hour	5 days

These results agree with experiments. For internal waves with wavelength λ = 10 km, the maximum amplitude A_{max} and stationary amplitude A_{st} in the case of exact resonance exceed 100 m, i.e., the waves emerge at the surface.

Brekhovskikh, L. M., V. V. Goncharov, V. M. Kurtepov, and K. A. Naugol'nykh. Interaction of internal and surface waves in the ocean. Okeanologiya, no. 2, 1975, 205-212.

The effect of nonlinear interactions between finite-amplitude surface and internal waves is described by use of a spectral method. The instability of resonant interaction between these waves is numerically analyzed, using spectral forms of expression for the complex wave amplitudes developed. The article includes a discussion on the advantages of the spectral form of the system of equations defining the complex amplitude of normal modes.

The essence of the spectral method is as follows. In a linear approximation, without allowing for any dissipation, the general solution of the wave equation system can be represented in the form of a superposition of normal modes, in which the amplitude of normal modes is independent of time. If it is assumed that the sum of normal modes is complete, the solution for the nonlinear case is found also in the form of a superposition of normal modes. However, in this case the amplitudes are time dependent, owing to dissipation and nonlinear interactions. The basic problem then is to develop and solve equations for the amplitudes of normal modes. These equations are called the spectral form of the initial equations in terms of partial derivatives.

One of the variants of the spectral method is the description of a nonlinear process by use of three- and four-wave resonant interactions. In this method, out of the entire spectrum of interacting waves only those waves which satisfy the condition of synchronism (sums of wave vectors and frequencies equal zero) are considered. The deficiency of the method is that in the case of interaction of waves with continuous spectra, neglect of a potentially large number of resonant and near-resonant interacting waves is difficult to justify, since they can affect the energy distribution between waves. This effect is called instability of resonant interactions, which can be self-induced during excitation of composite waves, if at the initial moment the amplitudes of the initial resonant wave system have non-zero values.

Instability of the resonant wave system with respect to small disturbances is possible as well. It occurs if at the initial moment, in addition to the amplitudes of the initial resonant wave system, the amplitudes of the other waves differ from zero. These two types of instability are analyzed, using as an example the interaction of surface and internal waves in the oceanic waveguide.

Bukatov, A. Ye. Internal waves generated in the sea with a density discontinuity layer, by periodic oscillations of a bottom sector. Morskiye gidrofizicheskiye issledovaniya, no. 1, 1974, 44-52.

In the present analysis, the undisturbed fluid density changes with depth according to

$$\rho(z) = \begin{cases} \rho_0 & -H_1 \le z \le 0 \\ \rho_0 \exp\left[-\kappa(z+H_1)\right] & -(H_1+H_2) \le z \le -H_1 \\ \rho_0 \exp\varepsilon & -H \le z \le -(H_1+H_2). \end{cases} \qquad (1)$$

where ϵ = kHz, ρ_0 = const. Periodic oscillations of a portion of the sea bottom are characterized by the vertical velocity

$$w^* = \alpha f(x,y) \cos \sigma t \tag{2}$$

As in the case of a two-layered sea (Bukatov, 1973), the problem is solved by the method of integral transforms.

The analysis shows that at $\sigma^2 > kg\,\sigma > 2\omega$ (2ω is Coriolis parameter), periodic oscillations of a portion of the sea bottom generate a single progressive wave, unattenuated in a two-dimensional geometry, but attenuated as $1/R^{\frac{1}{2}}$ in a three-dimensional geometry. For $4\omega^2 < \sigma^2 < kg$, an infinite, discrete spectrum of progressive waves is generated. The vertical distribution of the amplitudes of these waves is qualitatively equal to that in the case of the internal waves generated by periodic surface pressure; the phase velocities and wavelengths of the waves in these two cases are equal.

The effect of a large density gradient on w, u, and p of internal waves is illustrated in Figs. 1-3. The estimates are made for the function f(x) in the form

$$f(x) = \begin{cases} \cos^2 \pi x / 2\ell & |x| \le \ell \\ 0 & |x| > \ell \end{cases} \tag{3}$$

for $2\omega = 6.6 \times 10^{-5}$ sec, $\ell = 10^4$ m, $H_1 = 20$ m, $H_2 = 60$m, H = 2080 m, $0 \le \epsilon \le 5 \times 10^{-3}$, $2\omega < \sigma < 10^{-1}\ (0.5g/H_2)^{\frac{1}{2}}$

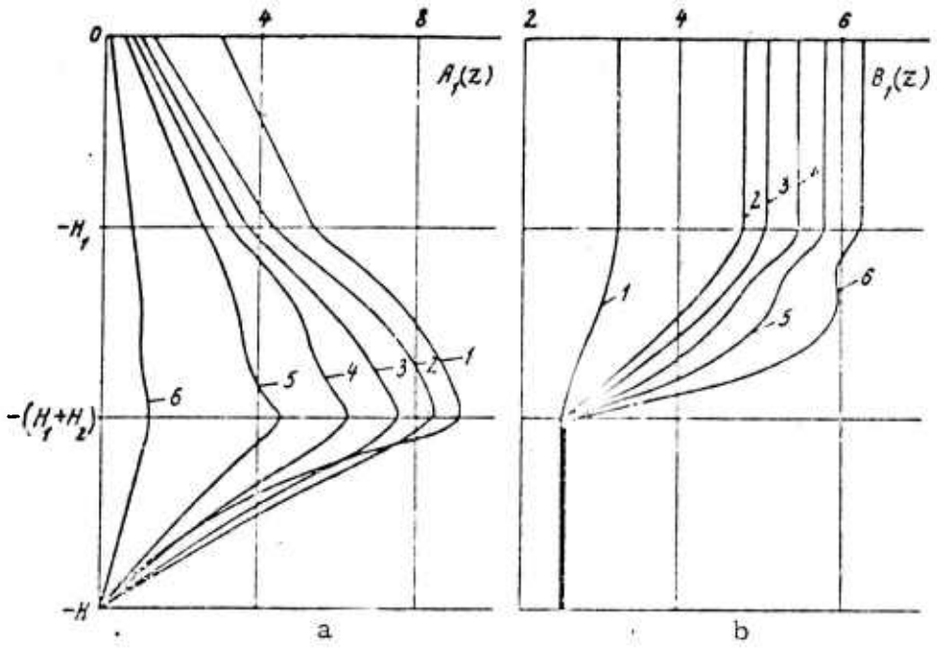

Fig. 1. $A_1(z) = 10^2 a^{-1} A(z)$ and $B_1(z) = a^{-1} B(z)$ (here $A = \max w$, $B = \max u$)

Curves 1-6: τ (hour) = 2; 4.8; 6; 8; 12; 24.

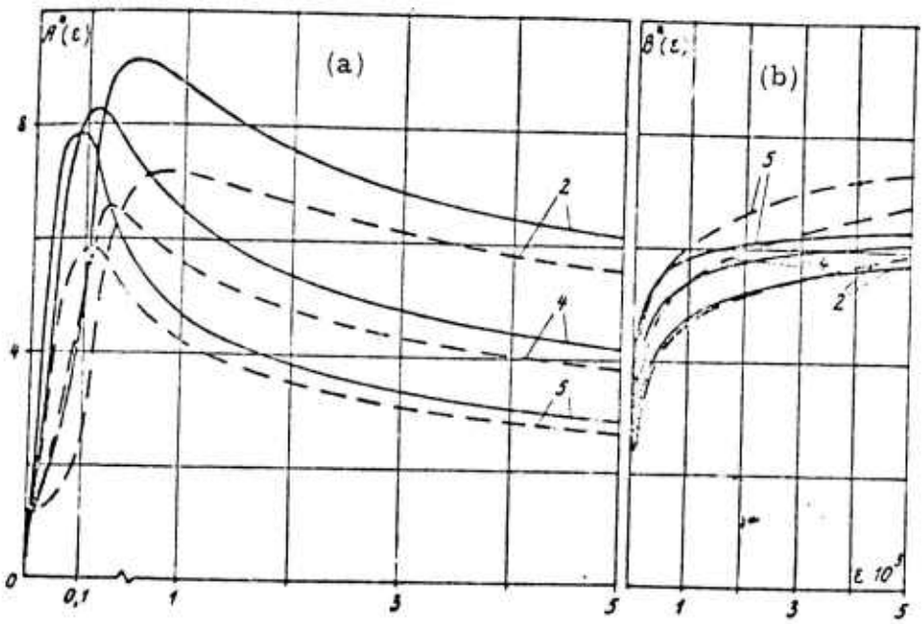

Fig. 2. Effect of density discontinuity on $A^* = 10^2 a^{-1} A(z)$ and $B^* = a^{-1} B(0)$.

Curves 2, 4, 5 - see Fig. 1. Dashed lines - results for two-layered ocean (Bukatov, 1973). Here z is the lower boundary of the density discontinuity layer.

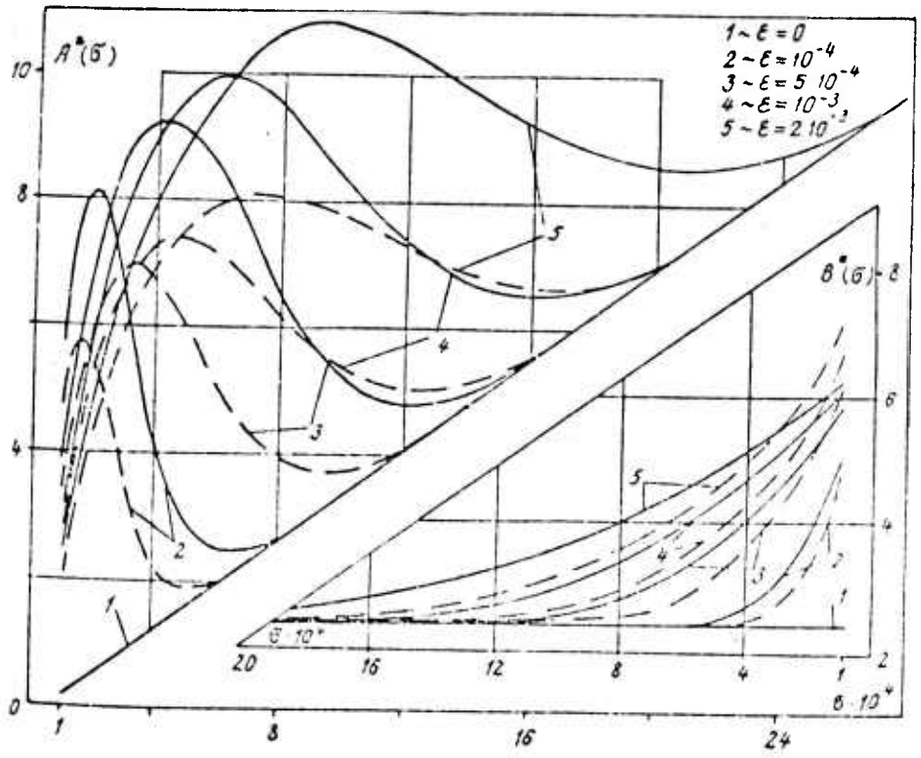

Fig. 3. Effect of oscillation frequency of the bottom on $A^* = 10^2 a^{-1} A(z)$ and $B^* = a^{-1} B(0)$ Dashed lines - the same as in Fig. 2.

Bukatov, A. Ye., and L. V. Cherkesov.
Effect of depth stratification on internal waves.
IN: Morskiye gidrofizicheskiye issledovaniya, no. 4, Sevastopol', 1974, 58-67.

Internal waves in a two-layer ocean generated by a pressure region $p_o = af(x, y)\cos\sigma t$ exerted upon the free surface are investigated. The undisturbed density of the water varies with depth according to:

$$\rho(z) = \begin{cases} \rho_0 \exp(-k_1 z) & -H_1 \le z \le 0 \\ \rho_1 \exp(-k_2 z) & -H \le z \le -H_1. \end{cases} \qquad (1)$$

where $\rho_1 = \rho_0 \exp[(k_1 - k_2)H_1]$.

The analysis of internal waves is made assuming that the motion of liquid in both layers can be described by the Fjeldstad equation system with boundary conditions $p - \rho g\xi = p_o$, $\xi_t = w$, at $z = 0$; $W = 0$ for $z = -H$, where p is the disturbed pressure, ξ is the deviation of the free surface from the undisturbed state, and W is the vertical velocity. In addition, continuity of W and hydrodynamic pressure at the interface is satisfied.

The results of the calculations indicate that two wave patterns are possible for $\sigma > 2\omega$ (2ω is Coriolis parameter).

For $\sigma \geq (\hat{k}g)^{1/2}$, where $\hat{k} = \max(k_1, k_2)$, only progressive surface waves are generated. Distortion of the parameters of the surface waves due to stratification factors ϵ_1 and ϵ_2 in two layers is negligible.

For $\sigma < (\hat{k}g)^{1/2}$, an infinite sum of waves is generated. When $k_1 < k_2$ ($k_1 \neq 0$), internal waves generated at frequenices $(k_1 g)^{1/2} \leq \sigma < (k_2 g)^{1/2}$ appear exclusively on account of the stratification factor of the lower layer (ϵ_2); they also appear if $k_1 = 0$. For $k_2 < k_1$ ($k_2 \neq 0$), internal waves generated for frequencies $(k_2 g)^{1/2} \leq \sigma < (k_1 g)^{1/2}$ appear on account of ϵ_1, and they also appear if $k_2 = 0$.

The results of numerical calculation are given in Table 1 and Figs. 1-3. Vertical and horizontal velocity components $\hat{A} = \sum_{n=0}^{\infty} |A(r_n, z)|$ and $\hat{B} = \sum_{n=0}^{\infty} \left|\frac{1}{r_n} A_z(r_n, z)\right|$ are analyzed for

$$f(x) = \begin{cases} \cos^2 \pi x / 2\ell & |x| < \ell \\ 0 & |x| > \ell, \end{cases} \qquad (2)$$

where $\ell = 10^4$ m.

As Fig. 1 shows, if $\epsilon_1 > 0$ and $\epsilon_2 \geq 0$, B^* is reached at the free surface, while A^* is reached within the ocean at depth h^*. For $\epsilon_1 = \epsilon_2 = 0$, $h^* = 0$; for $\epsilon_1 = 0$, $\epsilon \neq 0$, $h^* > H_1$; for $\epsilon_1 \neq 0$, $\epsilon_2 = 0$, $h^* = H_1$; and for $\epsilon_1 \neq 0$, $\epsilon_2 \neq 0$, $h^* > H_1$.

Table 1

Effect of stratification on wavelength of the first two harmonics of internal waves

$\epsilon_1 \times 10^3$ \ $\epsilon_2 \times 10^3$	0	0.1	0.5	1	2	5
0	- -	9387.1 4721.8	22671 11335	32371 16185	45906 23003	72769 36511
1	12289 4158.9	12895 9820.2	23003 13165	32539 16746	46176 23259	73023 36511
2	17444 5924.5	17740 9022.9	23609 16927	32879 18690	46176 23877	72938 36725
5	25665 9331.3	27788 9617.1	29209 21073	34316 26058	46865 28416	73193 37831

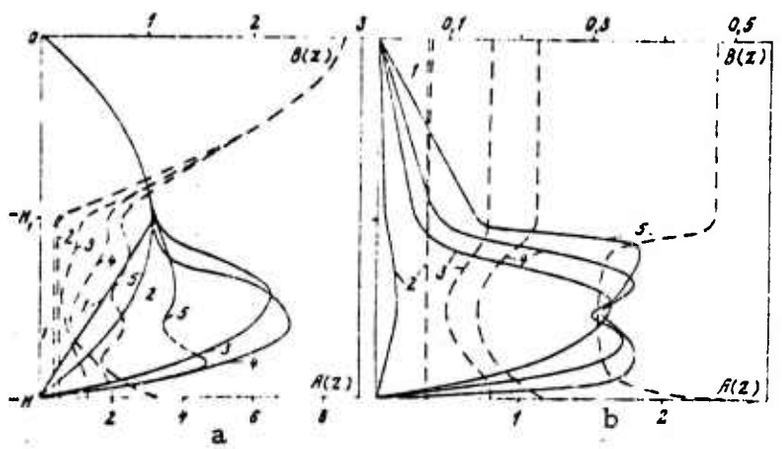

Fig. 1. $A = 10^4 \, a \, \bar{A}/\rho_0 g$ - solid lines and $B = 10^2 a \, \bar{B}/\rho_0 g$ - dashed lines calculated for $\epsilon_1 = 5 \times 10^{-3}$ (a) and $\epsilon_1 = 0$ (b), $\tau = 2\pi/\sigma = 6$ hour.

1- $\epsilon_2 \times 10^3 = 0$; 2- 0.1; 3- 0.5; 4- 1; 5- 5.

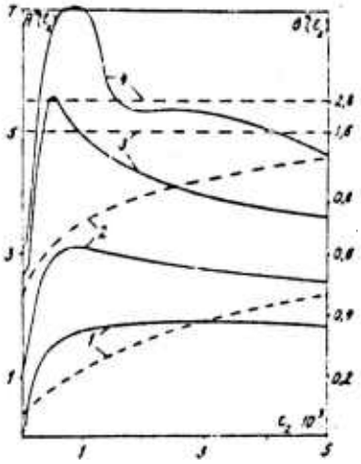

Fig. 2. $A^* = \max A(z)$ (solid lines) and $B^* = \max B(z)$ (dashed lines) calculated for $\tau = 6$ hours.

1 - $\epsilon_1 \times 10^{-3} = 0$; 2 - 1; 3 - 2; 4 - 5.

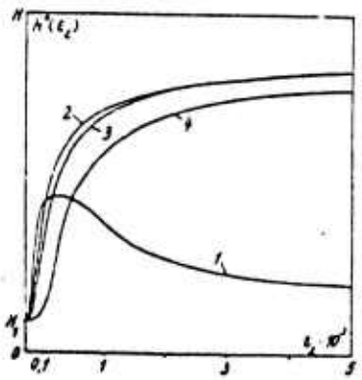

Fig. 3. Dependence of h^* on the stratification of the lower layer.

1-4 - same as Fig. 2.

Bukatov, A. Ye. Problem of internal waves in a continuously stratified sea. Morskiye gidrofizicheskiye issledovaniya, no. 3, 1973, 42-52.

Internal waves generated by periodic oscillations of a portion of the bottom of a continuously stratified sea are studied. The undisturbed fluid density changes with depth according to the relation

$$\rho(z) = \begin{cases} \rho_0 \exp(-\varkappa z) & -H_1 \le z \le 0 \\ \rho_0 \exp(\varkappa H_1) & -H \le z \le -H_1, \end{cases} \tag{1}$$

The sea bottom is assumed to oscillate with a vertical velocity given by

$$w^* = a f(x,y) \cos \sigma t . \tag{2}$$

The linearized system of equations of motion is then solved by the method of integral transforms. Expressions for disturbances of pressure, free surface, and interface at a large distance from the source, in the case of axisymmetric bottom oscillations, are found for two sets of conditions: $\sigma^2 > kg$, $\sigma > 2\omega$; and $2\omega < \sigma < (kg)^{1/2}$.

The results of the analysis show that the conditions for generation of internal waves by periodic oscillations of the ocean bottom are identical to those in the case of periodic surface pressure variations. For ($\sigma^2 > kg$, $\sigma > 2\omega$), only one surface wave is generated, and its amplitude decreases with depth. For $2\omega < \sigma < (kg)^{1/2}$ an infinite sum of waves is generated; the 0-th harmonic is an ordinary surface wave, while all higher harmonics are internal waves. The qualitative dependence of these waves on z is similar to that in the case of periodic surface pressure variations. The effect of an inhomogeneity of the fluid on w(z), u(z) and p(z) is illustrated in Figs. 1-3. These calculations are made for

$$f(x) = \begin{cases} \cos^2 \pi x / 2\ell & |x| \le \ell \\ 0 & |x| > \ell \end{cases} \tag{3}$$

and $2\omega = 6.6 \times 10^{-5}$ sec^{-1}, $\ell = 10^4$ m, $H_1 = 60$ m, $H = 2080$ m, $0 \leq \epsilon \leq 5 \times 10^{-3}$ and $2\omega < \sigma \leq$ (kg)$^{1/2}$.

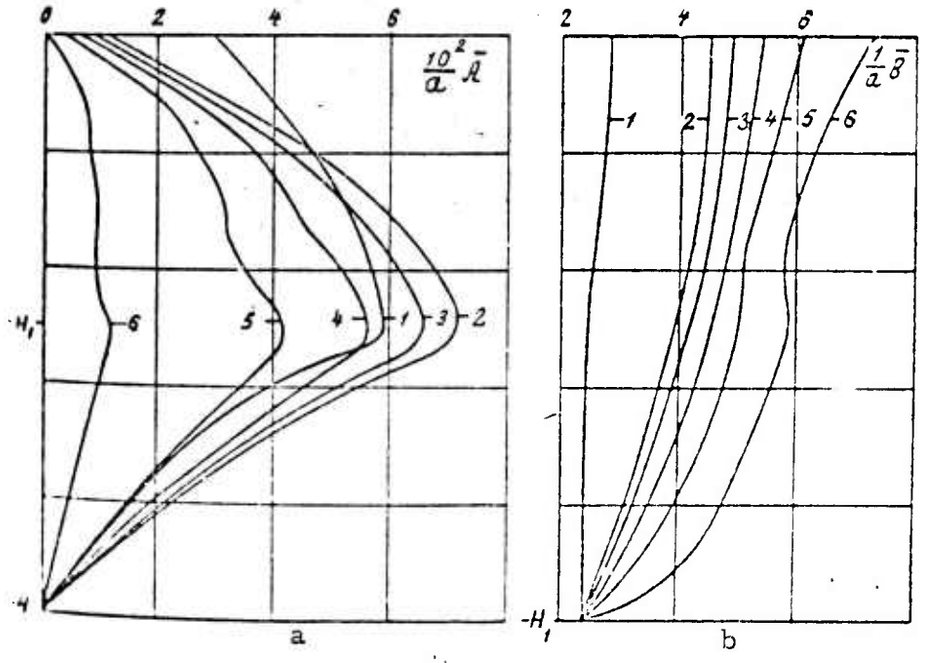

Fig. 1. Vertical distribution of $\bar{A}$ = max w and $\bar{B}$ = max μ.

Curves 1-6: $\sigma \times 10^4$ = 8.7; 3.625; 2.9; 2.175; 1.45; 7.25.

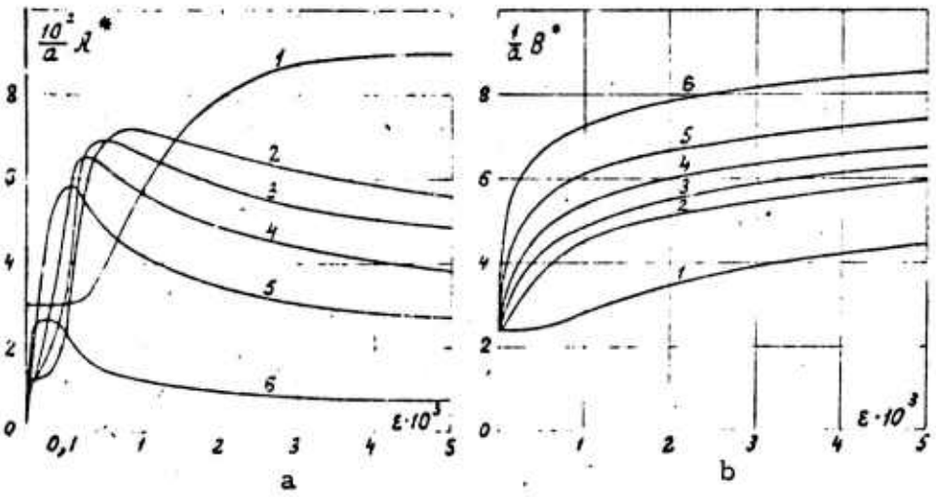

Fig. 2. Dependence of A^* = max $\bar{A}(z)$ and B^* = max $\bar{B}(z)$ on the stratification factor $\epsilon = kH_1$.

Curves 1-6: same as in Fig. 1.

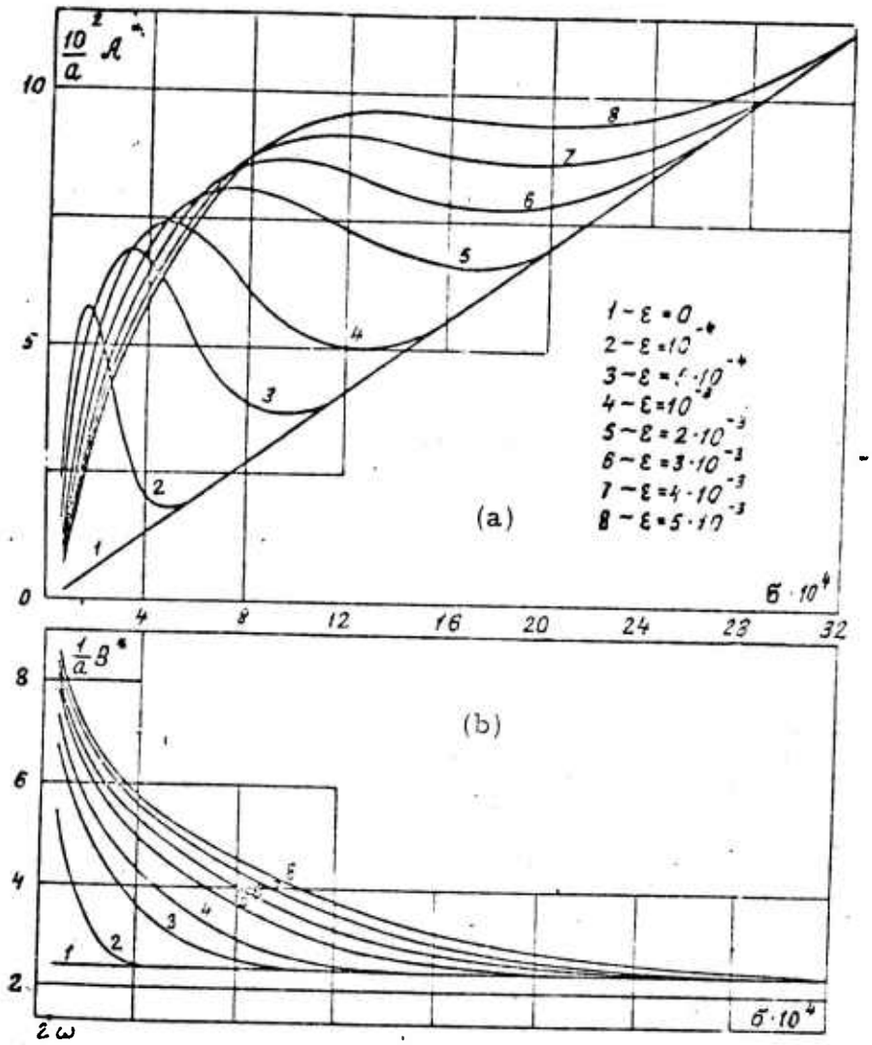

Fig. 3. Dependence of A^* and B^* on frequency of bottom oscillations.

The author notes that ice cover affects only short wavelength surface waves, just as in the case of internal waves generated by periodic surface pressure variations.

Chistyakov, A. I., and L. V. Rotermel'. On the dynamics of a towed stabilized system for underwater investigations. Trudy Kazanskogo aviatsionnogo instituta. No. 175, 1974, 50-55. (RZhVodnyy transport, 7/75, #7A60). (Translation)

The effect of the kinematic parameters of a towed system, having an intermediate lifting - stabilizing device, on its filtering properties is studied, for the case of ship roll. The results are represented in the form of graphs and are illustrated by an example.

Desnyanskiy, V. N. Spectral models of turbulence. Trudy VNII gidrometeorologicheskoy informatsii. Mirovoy tsentr dannykh. No. 8, 1975, 49-63. (RZhMekh, 8/75, #8B1041). (Translation).

Models describing the transfer of energy in terms of the spectrum of turbulent motions of various scales are examined analytically and numerically. Stationary regimes for these models are examined which for energy spectra in the inertial interval obey a (-)5/3 power law. It is shown that numerous models give a stationary regime of similarity. A series of numerical experiments with different spectral models are carried out. Periodic solutions for models with two quadratic integrals are obtained numerically.

Dotsenko, S. F. Effect of inhomogeneity of fluid and ice cover on waves generated by a moving pressure region. IN: Sb. Morskiye gidrofizicheskiye issledovaniya, no. 4, Sevastopol', 1974, 82-89.

The surface and internal waves in an ice-covered ocean with gradient layer, generated by a pressure region $p_o = af(x^* + vt)$ ($f(x^*) = 0$ at $x^* \geq \ell$) are investigated. The layer of an ideal incompressible liquid $-\infty < x^*, \overline{y} < +\infty$ with an elastic plate of thickness h = const, floating on its surface, is considered. The vertical profile of undisturbed density of fluid is described by

$$\rho_0 - \rho_1 \begin{cases} 1, & -h_1 \leq z \leq 0, \\ \exp\left[-k\left(z + h_1\right)\right], & -h_1 - h_2 \leq z \leq -h_1, \\ \exp \epsilon, & -H \leq z \leq -h_1 - h_2 \end{cases} \tag{1}$$

where $k \geq 0$, $\epsilon = kh_2$.

An expression for vertical velocity field w(x, z) in the case when f(x) is an even function, is obtained in the form

$$w = \theta(x)\left[w_n(x,z) + w_B(x,z)\right] + w_0(x,z), \tag{2}$$

where θ is the Heaviside function, $W_o \longrightarrow \infty$ when $x \to \infty$; W_n corresponds to unattenuating surface waves, and W_B corresponds to internal waves.

An analysis of W_n and W_B shows that the presence of an ice cover does not cause a qualitative change in the structure of W_B, but only to change in velocities. As in the case when ice cover is absent (h = 0), n-1 internal waves are generated at $V_{n+1} < V < V_n$. However, the presence of ice cover does lead to a qualitative change in the structure of the W_n field. In the case of solid ice cover ($E \neq 0$, $h \neq 0$) two surface waves are generated

at $V_0 < V$, two surface waves are generated at $V_o < V < V_1$, and one surface wave is generated at $V > V_1$. In the presence of broken ice cover ($E = 0$, $h \neq 0$) no waves are generated at $V > V_1$, while one wave is generated at $V < V_1$. The wave generated at $V > V_1$ as well as one of the waves generated at $V_0 < V < V_1$ are caused exclusively by the elastic properties of the ice (elastic waves).

Numerical analysis of internal waves is made for two cases: concentrated and distributed pressure p_0. It shows that changes in internal wave field induced by ice cover are insignificant, and they arise only due to the inertial properties of the ice cover.

A numerical analysis of the effect of fluid inhomogeneities on surface waves is performed, using the following expression for V_0 developed for $H = +\infty$, $\rho_0 = \text{const}$, and $\rho = 0$ (Kheysin, 1963; 1967):

$$V_0 = 1.325\,(dg/\rho_o)^{1/8} \tag{3}$$

The results of the analysis are shown in Figs. 1-4. The effect of fluid inhomogeneities on surface waves is insignificant. It is highest at $V \to V_0 + 0$ for elastic waves, and at $V \to V_1 - 0$ for gravity waves.

As Fig. 1 illustrates, in the presence of an elastic ice cover, the (V, h) domain is divided into five regions with qualitatively different wave motions: 1) $V > V_1$ - only elastic surface waves originate; 2) $\max(V_0, V_2) < V < V_1$ - elastic and gravity surface waves originate; 3) $V_2 < V < V_0$ - no unattenuating waves originate; 4) $V_0 < V < V_1$ - elastic and gravity surface waves and internal waves originate; and 5) $V_0 < V < \min(V_0, V_2)$ - only internal waves originate.

Hence the combined action of an elastic ice cover and fluid inhomogeneities results in a wave motion which is considerably different both from the one which originates in a homogeneous liquid with ice cover, and from one in an inhomogeneous liquid without ice cover. The wave motion which originates in an inhomogeneous fluid with a broken ice cover is analogous to that in a homogeneous liquid with no ice cover.

The wave field in an inhomogeneous liquid with an ice cover, generated by a moving pressure, can be approximated by $\overline{w} = w_n \Big|_{k=0} + w_B \Big|_{h=0}$.

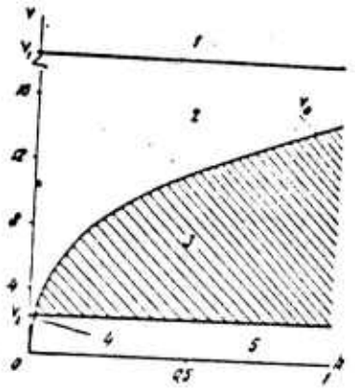

Fig. 1. Calculations of $V_0(h)$ for: $h_1 = 20$ m, $h_2 = 10^2$ m, $H \cong 2 \times 10^3$ m, $\epsilon = 10^{-2}$, $\rho_1 = 10^3$ kgm^{-3}, $E = 3 \times 10^3$; $\sigma = 0.34$, $\rho = 870$ kgm^{-3}, $0 < h < 5$ m.

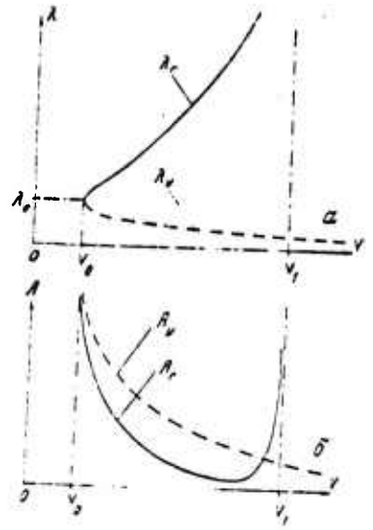

Fig. 2. Schematic dependence of wavelengths and amplitudes on V for elastic (dashed line) and gravity surface waves (solid lines) in the case of a concentrated moving pressure.

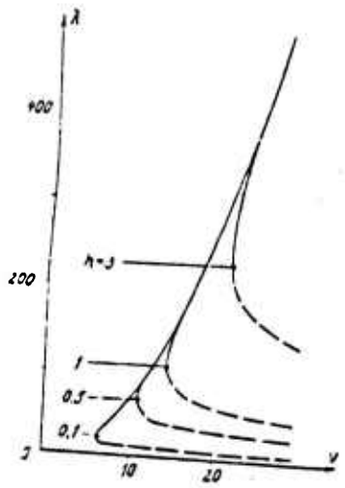

Fig. 3. Dependence of wavelengths on V for elastic and gravity surface waves for various h.

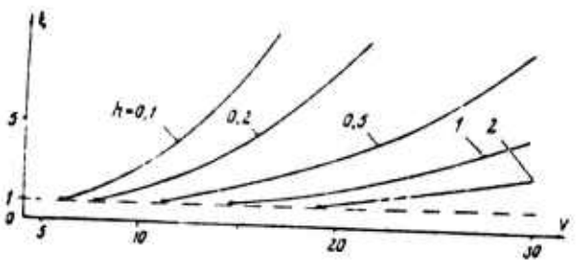

Fig. 4. Dependence of the ratio between amplitudes of elastic and gravity surface waves on V for various h.

Dotsenko, S. V., A. N. Nedovesov, M. G. Poplavskaya, and V. A. Ryzhenko. Spatial-spectral characteristics of remote sensors. IN: Sb. Morskiye gidrofizicheskiye issledovaniya no. 2(65). Sevastopol', 1974, 162-173.

An analytical expression is developed for the spatial-spectral characteristic of a remote sensor (i. e. dependence of its transfer function on wave number), which is intended for aircraft and satellite measurements of physical fields in the ocean surface. The analysis assumes that a) the measured surface physical field is homogeneous, isotropic, and "frozen"; b) the sensor has axial symmetry, with directional pattern and aperture function independent of azimuth, and its directional pattern is sufficiently narrow so that equality between the shape of directional pattern and aperture function is valid; c) the sensor is a fast-response type and linear. Using the expressions developed, the authors provide numerical calculations for a sensor with uniform averaging, and specifically for sensors of the radiometers aboard the Cosmos-149 and Tiros-2 satellites.

The general form of the spatial-spectral characteristic is

$$K_1(\alpha)=\frac{S_{np}(\alpha)}{G_1(\alpha)}=M_e(\alpha,0)-\int_0^\infty F_1(\alpha,\varkappa)\frac{G_1\left(\sqrt{\varkappa^2+\alpha^2}\right)}{G_1(\alpha)}\,d\varkappa. \qquad (1)$$

where $\alpha = \omega / V_o = 2\pi/\lambda$, $M_\ell(\alpha, 0)$ and $F_1(\alpha, x)$ are functions of longitudinal and transverse averaging, and $G_1(\alpha)$ is the spectrum of the measured field.

After introducing the nondimensional variable $y = \alpha R = 2\pi R/\lambda$ (R is radius of aperture function) and the spectrum for the field having the autocorrelation function $B_X(r) = \sigma^2 \exp(-\beta r)$, where σ^2 is variance for field fluctuations, equation (1) becomes

$$K(y)=M_1(y)-\int_0^\infty F(y,x)\frac{z^2+y^2}{z^2+y^2+x^2}\,dx, \qquad (2)$$

where $z = \rho R$ represents the ratio between the radius of the aperture function of the sensor and the spatial scale $1/\beta$ for the field.

Aperture functions and the results of calculations for various remote sensors are given in Figs. 1-3 and Table 1. Table 1 illustrates the remote sensor capabilities from an aircraft flying at h = 10 km.

Table 1

Apparatus →	Wide-angle radiometer of Tiros-2	Five-channel radiometer of Tiros-2	Radiometer, Cosmos-149
directional pattern width	48° 16'	5° 04'	2° 26'
Diameter of radiation area d, km	8.93	0.87	0.42
$\lambda_{0.5}$, km	26.2	3.66	2.75
$\lambda_{0.3}$, km	19.0	2.64	1.95

Note: $\lambda_{0.5}$ and $\lambda_{0.3}$ are the periods of the spatial inhomogeneities of a field for which K (y') = 0.5 and K (y') = 0.3.

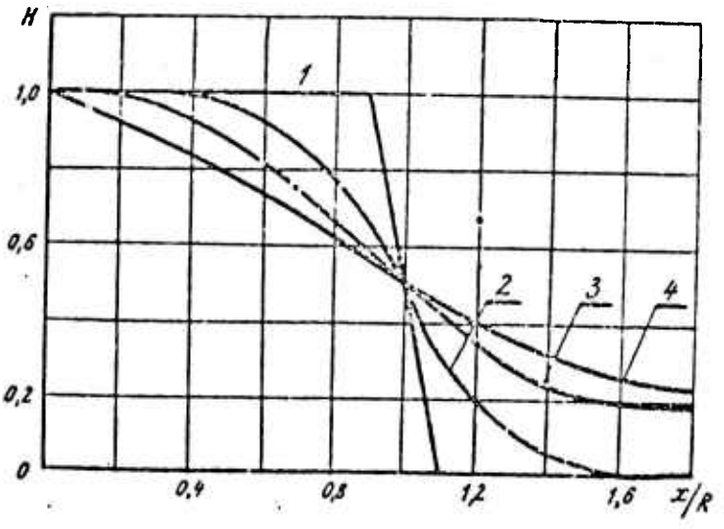

Fig. 1. Normalized aperture functions.

1- sensor with uniform averaging; 2- sensor of wideangle radiometer of Tiros-2; 3- sensor of Tiros-2 five-channel radiometer; 4- sensor of Cosmos-149 radiometer.

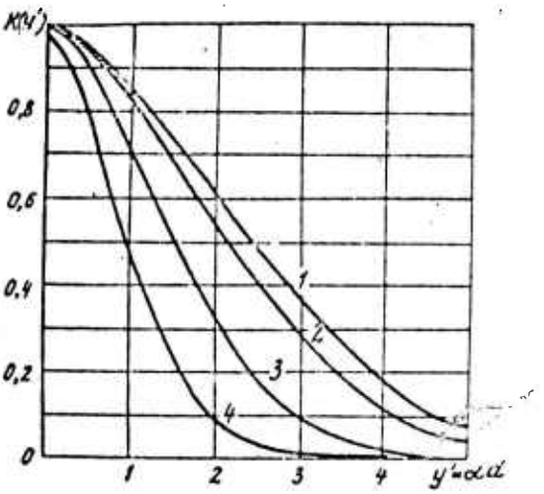

Fig. 2. Normalized spectral characteristics (d is diameter of radiation area); 1-4 - as in Fig. 1.

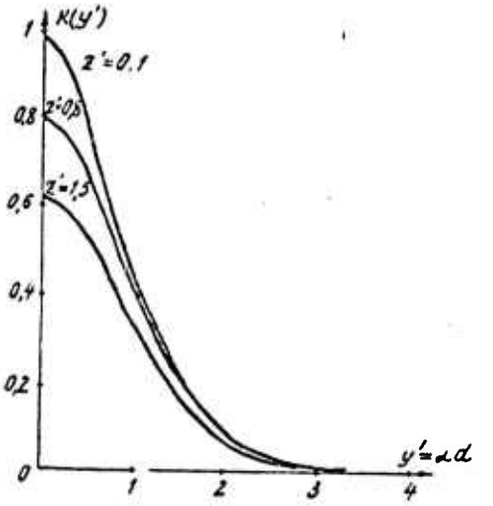

Fig. 3. Spectral characteristics for various $z' = \beta d$; 1-4 - as in Fig. 1.

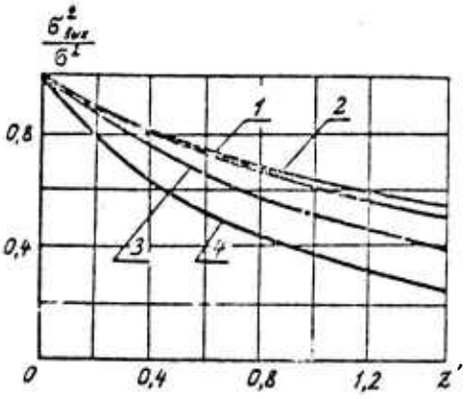

Fig. 4. Dependence of power attenuation factor for output signal on $z' = \beta d$. 1-4 as in Fig. 1.

Dotsenko, S. V. Reconstruction of physical field values in the ocean from the results of their measurement on rectilinear trajectories. IN: Sb. Morskiye gidrofizicheskiye issledovaniya no. 2(65). Sevastopol', 1974, 148-161.

The optimal reconstruction of a two-dimensional homogeneous "frozen" scalar field X (x, y) at the point (r, 0), from a one-dimensional random realization X (0, y) of that field, is discussed. The reconstruction is based on the principle of least square error. The problem is reduced to finding the aperture function H(y) which minimizes the mean square error under the condition that $\int_{-\infty}^{\infty} H(y)\,dy = 1$. The aperture function H(y) is determined by the Ritz method. The solution obtained is applied in the analysis of physical fields with spectra in the form (Monin and Yaglom, 1967):

$$S_0(\rho,\omega)=\sigma^2\frac{\Gamma(p+\frac{1}{2})}{\sqrt{\pi}\,\Gamma(p)}\cdot\frac{\alpha^{2p}}{(\alpha^2+\omega^2)^{p+1/2}}\,. \qquad (1)$$

where Γ (p) is the gamma function; and $\alpha=\frac{\varkappa_p}{L_x}=\frac{2\varkappa_p}{\pi}\Omega_x$, where $\varkappa_p=\sqrt{\pi}\,\frac{\Gamma(p+1/2)}{\Gamma(p)}$. Expressions for optimum aperture function for p = 1/3, p = 1/2, and p→∞ were found (see Fig. 1).

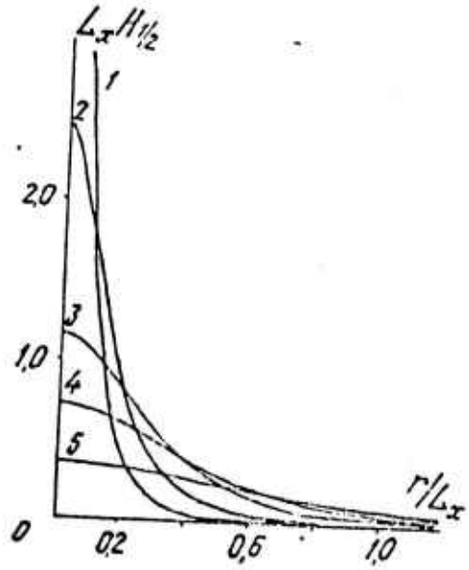

Fig. 1. Aperture functions for p = 1/2.
1- $\gamma = r/L_x$ = 0.1; 2- 0.2; 3- 0.4; 4- 0.6; 5- 1.0.

The results of this analysis indicate that more measurement points should contribute in the reconstruction of the field at point (r, 0) as this point becomes more distant from the trajectory. Optimum reconstruction of a field from measurements along a rectilinear trajectory is possible within a rather narrow band (narrow in comparison to the characteristic scale L_x). With an allowable error of 30%, that band is bounded by $r = 0.02\ L_x$ for $p = 1/3$, $r = 0.060\ L_x$ for $p \to \infty$.

The gain in accuracy of reconstruction of the field from measurements along a trajectory, as compared to accuracy of reconstruction from measurement at a point, is independent of γ for $\gamma \ll 1$, and is given by

$$\mu = \sqrt{\frac{2\Gamma(p+1/2)}{\sqrt{\pi}\,\Gamma(p+1)}} \qquad (2)$$

where $0 < p < 1$.

The author concludes that reconstruction of a field from measurements along rectilinear trajectories has merit for nondifferentiable fields. At small $\gamma = r/L_x$ this reconstruction yields considerable gain in accuracy as compared to reconstruction from measurement at a point.

Gusev, A. V., and A. P. Polyakov. Vibration of measuring systems submerged in a flow during investigations of ocean microstructure. Trudy Arkticheskogo i Antarkticheskogo NII, no. 324, 1974, 126-133. (RZhGeofiz, 5/75, #5V12). (Translation)

Results are given of theoretical and experimental studies on vibration of a measuring system submerged in a flow. The sources of vibrations are analyzed and forces inducing vibration in elements of a measuring system (cables, ropes, rods) are estimated. Theoretical analysis shows that

a decrease in diameter of extended cylindrical elements, damping of rotational motion of these elements, addition of more suspension points, and provision for independent separation of vortexes along extended elements, are all needed to minimize vibrations.

Experimental studies of vibrations of a system in a flow, made using a 3-axis vibration pick-up, confirm that the most intense vibrations are those in the direction normal to the flow direction; they exceed longitudinal and vertical vibrations by an order of magnitude. A comparison of vibration amplitudes for different measuring systems shows that at some frequencies they differ by more than factor of 1000. The results of experimental studies also confirm the conclusion that with an increase in the diameter of a cable, the intensity of vibrations increases and that a system which is analogous to a string has a higher noise stability than a thread with distributed mass. Recommendations are made on the selection of optimal measuring systems for use in the study of various ocean parameters, particularly for fine microstructures.

Isayev, I. L., and Yu. P. Lomanov. Effect of meteorological conditions on the structure of the ocean surface temperature field. Morskiye gidrofizicheskiye issledovaniya, no. 2, 1974, 110-120.

The spectral characteristics of mesoscale surface temperature inhomogeneities, as functions of mean wind velocity and temperature, are analyzed for stationary conditions. The results are compared to experimental findings, in which measurements of the surface temperature were made by towed temperature sensors in the Northern and Tropical Atlantic along tracks exceeding 10,000 miles in length. Spectral densities of temperature inhomogeneities, normalized by dispersion, are calculated from 16 series with a sampling interval of 0.5 mile (see Table 1).

Table 1

Normalized spectral density E_N for various values of wind velocity

V, m/sec	$\overline{V}$, m/sec	E_N for various scales (in m)								Mean slope
		50	30	20	15	10	7	5	3	
8-10	9.2	1.3×10^6	3.3×10^5	9.1×10^4	4.9×10^4	1.2×10^4	4×10^3	1.7×10^3	5×10^2	-2.95
5-7	6.25	10^6	3.3×10^5	1.2×10^5	6.3×10^4	2.1×10^4	8.1×10^3	4.2×10^3	1.4×10^3	-2.37
3-5	4	10^6	2.8×10^5	1.2×10^5	7×10^4	3.1×10^4	14×10^3	6.9×10^3	3×10^3	-2.22
2-3	2.6	8.9×10^5	3.5×10^5	1.3×10^5	7.5×10^4	3.8×10^4	1.8×10^3	7.9×10^3	2.8×10^3	-2.07
≤ 2	≤ 2	7.5×10^5	3.4×10^5	1.6×10^5	9×10^4	3.7×10^4	1.8×10^3	10^4	3.7×10^3	-1.96

The equation for spectral density is obtained by adding terms to the Corsin equation in spectral form, integrated over wave numbers which allow for decay and generation of temperature inhomogeneities. The modified equation is then solved for $k \geq k_o$ using Pao's expression for the energy transfer $W(k)$ across point k.

The analysis shows that the main factors governing the temperature field are evaporation and heat exchange through the atmosphere, and they are consequently accounted for in further analysis. The shape of the spectral density curves for temperature inhomogeneities in the 3-50 km scale range are analyzed, using the derived solution and assuming that the production of inhomogeneities is absent and that molecular dissipation is negligible.

An expression for spectral density is developed in the following form:

$$E_\kappa = \frac{W_0(\kappa_0)^{\frac{2\lambda}{\rho c p \gamma \varepsilon^{1/3}}}}{} \kappa^{-\left(\frac{5}{3} + \frac{2\lambda}{\rho c p \gamma \varepsilon^{1/3}}\right)} \qquad (1)$$

where exponent of k can be expressed as

$$-\left(\frac{5}{3}+\frac{2\lambda}{\rho c\beta\gamma\varepsilon^{1/3}}\right)=-\left(\frac{5}{3}+\frac{3{,}52\cdot 10^{6}V}{\rho c\beta\gamma\varepsilon^{1/3}}\right)=-\left(\frac{5}{3}+\alpha V\right). \qquad (2)$$

where V is wind velocity. From experimental data $\alpha = 1.38 \pm 0.7$ sec/cm.

The depth of the temperature inhomogeneities is given by

$$h = \beta_1 L^{2/3} = \beta K^{-2/3} \qquad (3)$$

When corresponding values for γ, ρ, and C are inserted in eq. (2), we obtain $\beta = 2.87 \times 10^{-3}\ \epsilon^{-1/3}$. For scales within the 3-50 km range, $10^{-5} \leq \epsilon \leq 10^{-3}$. Hence $2.87 \times 10^{-2} \leq \beta \leq 13.4 \times 10^{-2}$, and for L = 10 km the depth of inhomogeneity is $85 \leq h \leq 400$ cm.

The dependence of the normalized spectral density on wind velocity for various scales of temperature inhomogeneities is shown in Fig. 1.

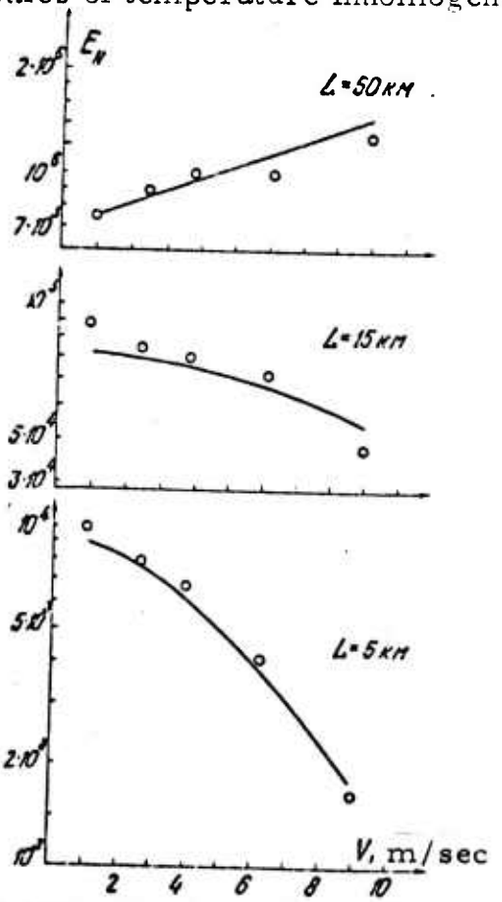

Fig. 1. Dependence of normalized spectrum E_N on wind velocity for various scales of temperature inhomogeneities k.

Kalatskiy, V. I. Numerical solution of a system of equations for turbulent motion of the upper ocean layer. Trudy Gidrometeorologicheskiy n.-i. tsentr SSSR. No. 119, 1975, 61-69. (RZhMekh, 8/75, #8B601). (Translation)

The problem of calculating nonstationary temperature distribution in the upper oceanic layer during its warming is considered. A numerical calculation scheme is proposed for solution of the system of equations for the turbulent boundary layer in the ocean. The system consists of equations of motion, thermal conductivity, turbulent energy balance and Kolmogorov relations which close the system. Two numerical schemes, one for a near-surface and the other for a deeper layer, are proposed for the solution of the turbulent energy balance equation.

The calculations show that the proposed system enables one to calculate the main parameters of the temperature structure in the upper ocean layer.

Kolesnikov, A. G., V. M. Kushnir, and N. A. Panteleyev. Time variation in the mean energy of small-scale turbulent fluctuations. FAiO, no. 8, 1975, 869-873.

Measurements and analysis were carried out aboard the R/V Akademik Vernadskiy to study the temporal variation of variance for u, v, w, and θ within a 0.1-15 meter range. The corresponding range of 95% confidence limits is analyzed in real time using formulas

$$S_v^2 = \frac{1}{m-1}\sum_{i=1}^{m}\left(z_{i+v} - \frac{1}{m}\sum_{i=1}^{m} z_{i+v}\right)^2,$$

$$\theta_{wv} = \frac{S_v^2}{1+\sqrt{2/m}\,q_{1-P}}, \quad \theta_{Nv} = \frac{S_v^2}{1+\sqrt{2/m}\,q_P}, \quad P = \frac{1}{2\pi}\int_{-\infty}^{q_P} e^{-t^2/2}\,dt, \tag{1}$$

where z_i are discrete values of the fluctuating parameter, P is probability of the confidence limit estimation, q are quantiles of normal density function, and $m > 50$. Typical results are given in Figs. 1-3.

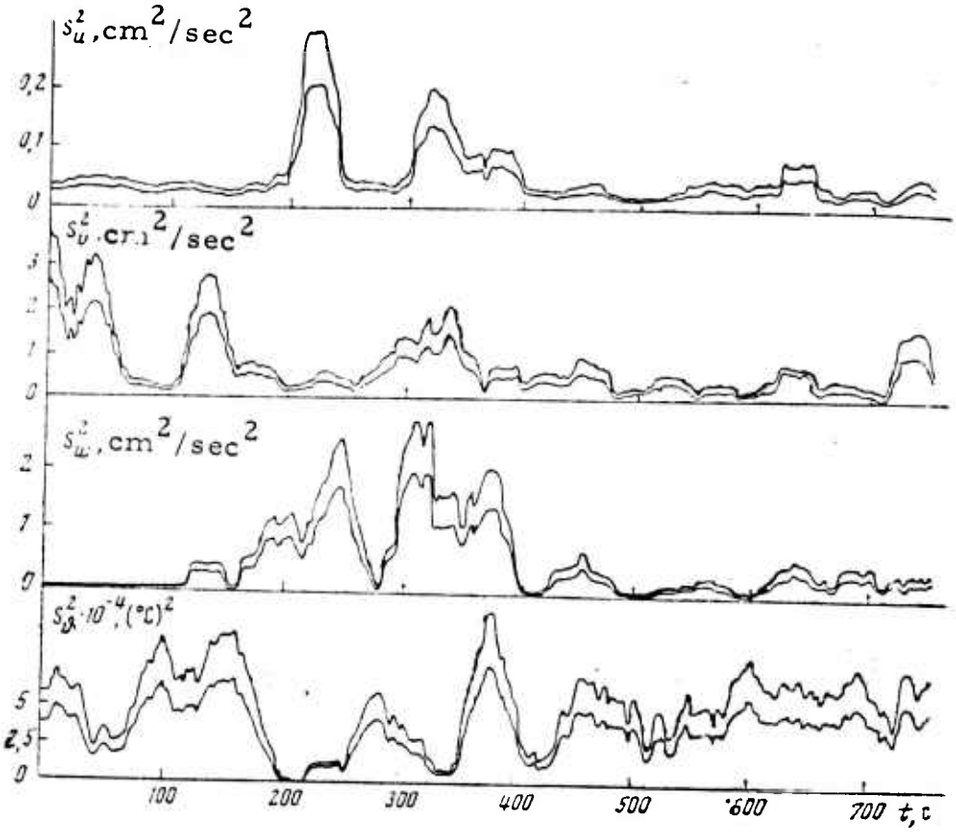

Fig. 1. Limits of 95% - confidence interval for variance of velocity components and temperature, measured in the Mozambique Straits.

Fig. 2 shows results obtained in the Caribbean Sea under the following conditions: measurement depth is 310 m; $\partial T / \partial z \sim 0.002\text{-}0.03^{\circ}$ C/m; $\partial \rho / \partial z \sim 0.3 \times 10^{-2}$ cond. unit/m; $\partial U / \partial z \sim 1 \times 10^{-3}$ sec^{-1}; Ri = 20-30; σ_u = 1-2.5 cm/sec; σ_v = 2-5 cm/sec; σ_w = 0.7-5 cm/sec. Fig. 1 shows results obtained in the Mozambique Straits under the following conditions: measurement dpeth is 250 m; $\partial T / \partial z \sim 0.01\text{-}0.02^{\circ}$ C/m; $\partial \rho / \partial z \sim 0.01$ cond. unit/m; $\partial U / \partial z \sim 0.5 - 1 \times 10^{-4}$ sec^{-1}; Ri = 2000-3000; σ_u = 0.05-0.6 cm/sec; σ_v = 1-2 cm/sec; σ_w = 0.6-2 cm/sec.

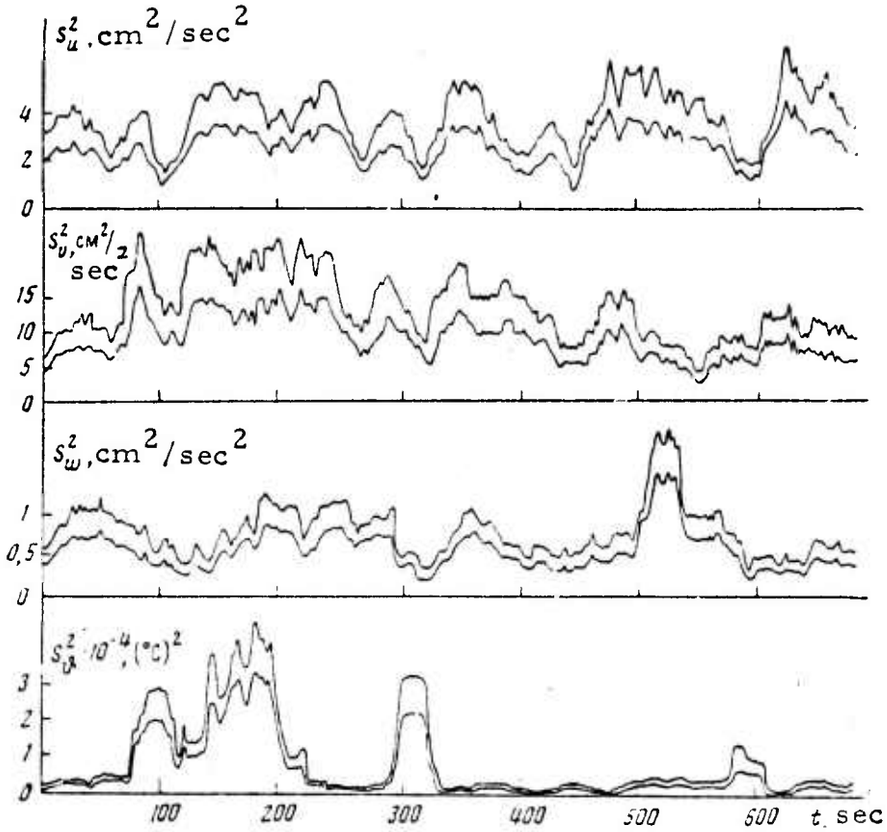

Fig. 2. The same as Fig. 1, for the Caribbean Sea.

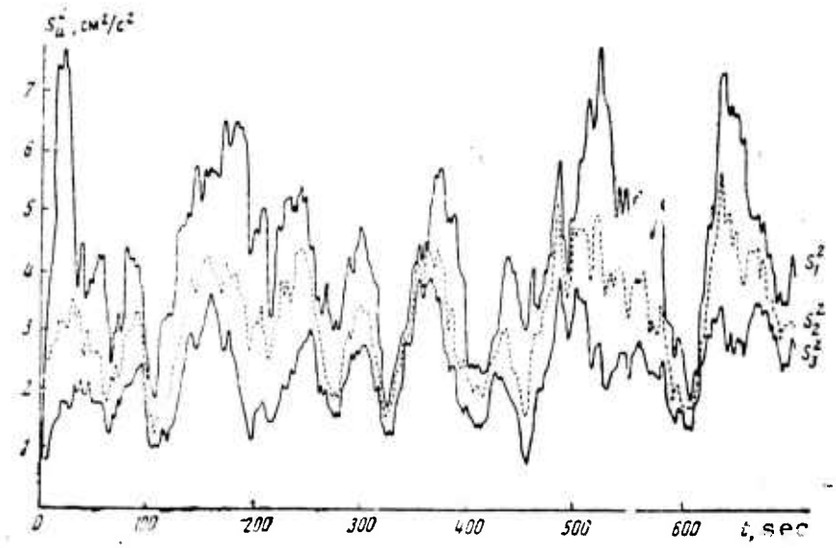

Fig. 3. s_u^2 calculated for various scale ranges: 1 - 15-0.1 m; 2 - 4-0.1 m; 3 - 2-0.1 m.

Figs. 1 and 2 illustrate inverse variation patterns for s_θ^2 on the one hand and S_u^2, S_v^2 and S_w^2 on the other hand. The decay of temperature inhomogeneities on the areas of intense velocity fluctuations is offered as a possible explanation of these variation patterns. The results given in Fig. 3 are explained as indicating that variation in the mean energy of small-scale turbulence is due to an uneven inflow of energy from large-scale fluctuations.

It is pointed out that intermittency of oceanic turbulence has a structure more complex than the one based on the concept of local areas with a more or less homogeneous intensity level of fluctuations.

Konyayev, K. V. Measuring the spatial structure of internal waves in the ocean, using a gradient system of temperature sensors. FAiO, v. 11, no. 7, 1975, 734-742.

Theoretical and experimental data are presented on a gradient sensing system for determining spatial spectra of internal waves.

The article includes a description of: 1) a gradient system of temperature sensors for measuring two-dimensional energy spectrum $\hat{g}(\varphi, f)$ and dispersion $\hat{\rho}^2(f)$ of a random wave field $\xi(x, y, t)$; 2) an algorithm for estimating $\hat{g}(\varphi, f)$ from the measured wave field $\xi_1(t) = \xi(0, 0, t)$, and two gradients: $\xi_2(t) = \partial\xi/\partial x\big|_{x=0,\ y=0}$ and $\xi_3(t) = \partial\xi/\partial y\big|_{x=0,\ y=0}$; 3) the form of the spectral window of the gradient system; 4) the response of the gradient system to standing internal waves; and 5) an experiment and its results pertaining to the Caspian Sea.

The gradient system consists of five distributed-type temperature sensors placed at the four corners and center of 2-m-diagonal square (see Fig. 1). The sensor in the center measures $\xi_1(t)$, while two pairs of sensors at the corners measure $\xi_2(t)$ and $\xi_3(t)$. The linear dimension

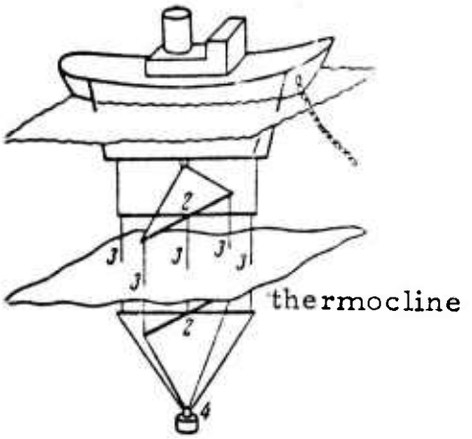

Fig. 1. Gradient system of temperature sensors, lowered from a ship.

1 - horizontal support bar; 2 - rigid cross pieces; 3 - distributed temperature sensors; 4 - weight.

of the gradient system (lm) is an order of magnitude smaller than the wavelength of the measured waves. Due to its underlying principle, the gradient system is applicable only for measuring weak waves.

An algorithm for calculation of the two-dimensional energy spectra is developed in the form

$$\hat{g}(\varphi, f) = \frac{1}{2\pi}\left\{g_{11}(f) + \frac{1}{\pi\rho}\operatorname{Im} g_{12}(f)\cos\varphi + \frac{1}{\pi\rho}\operatorname{Im} g_{13}(f)\sin\varphi + \right.$$
$$\left. + \frac{1}{2\pi^2\rho^2}[g_{22}(f) - g_{33}(f)]\cos 2\varphi + \frac{1}{\pi^2\rho^2}\operatorname{Re} g_{23}(f)\sin 2\varphi\right\}, \quad f \geqslant 0. \tag{1}$$

while dispersion is expressed by

$$\hat{\rho}^2(f) = \frac{g_{22}(f) + g_{33}(f)}{4\pi^2 g_{11}(f)}, \tag{2}$$

where $g_{nm}(f)$ are cross-spectra for $\xi_1(t)$, $\xi_2(t)$ and $\xi_3(t)$, ρ and φ are modulus and direction of the wave vector.

Analysis of the properties of the spectral window shows that the available frequency range is limited both at the low and high frequency ends. While the upper limit can be easily determined from the parameters of the system, the determination of the lower limit is more complicated. The spectral window is peculiar by its frequency-independent $\Delta\varphi$. Its area $\Delta f f \Delta\varphi$ decreases when approaching the origin of coordinates, i.e., the resolution of the analysis is enhanced. The spectral window contracts with a decrease of f, hence the intensity of reconstruction of $\xi(x, y, t)$ changes over the frequency range (5 at the upper limit, 17 at the lower limit, and 6-11 around the spectral density peak).

Analysis of the response of the gradient system to the standing waves

$$\xi_1(x, y, t) = \cos 2\pi (k_0 x + l_0 y - f_0 t) + \cos 2\pi (k_0 x + l_0 y + f_0 t) \qquad (3)$$

shows that the estimate of $\hat{g}(\varphi, f)$ and $\hat{\rho}(f)$ depends on the position of the gradient system (on $\alpha = k_0 x_0 + l_0 y_0$). Expressions are given for $\hat{g}(\varphi, f)$ and $\hat{\rho}(f)$ when standing waves propagate along the x-axis and the gradient system is placed at different points (at 2π $2k_0 x_0 = 0$; $\pi/2$, or $3\pi/2$, and π).

Experiments of this type were performed in the Caspian Sea in 1972 with the gradient system at a depth of 17 m (thermocline). Signals $\xi(t)$ very often have regular quasisinusoidal form. The results of calculations are shown in Figs. 2-4.

It is concluded that the gradient system of temperature sensors can be used for uniquely estimating the two-dimensional spectrum and dispersion for one mode. It is suitable for experiments in the open sea. However, high and nonuniform errors with respect to frequency hinder interpretation of results.

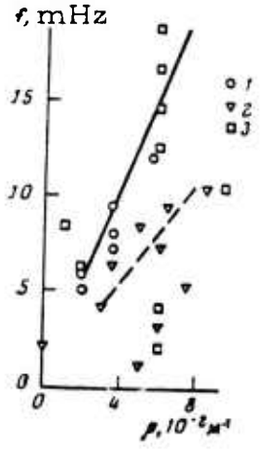

Fig. 2. Dispersion relation from data of T-shaped sensor array (1) and gradient system (2, 3).

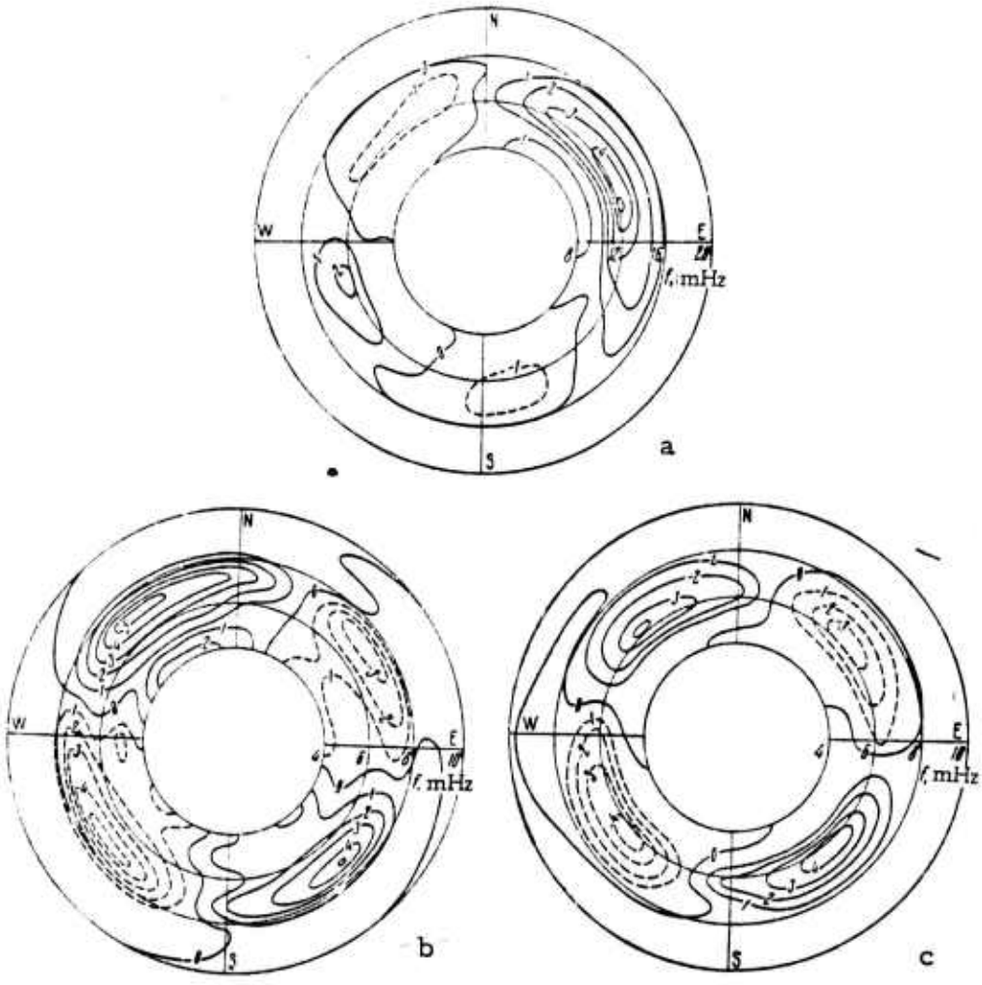

Fig. 3. Two-dimensional spectra $\hat{g}(\varphi, f)$ for progressive (a) and standing (b, c) internal waves.

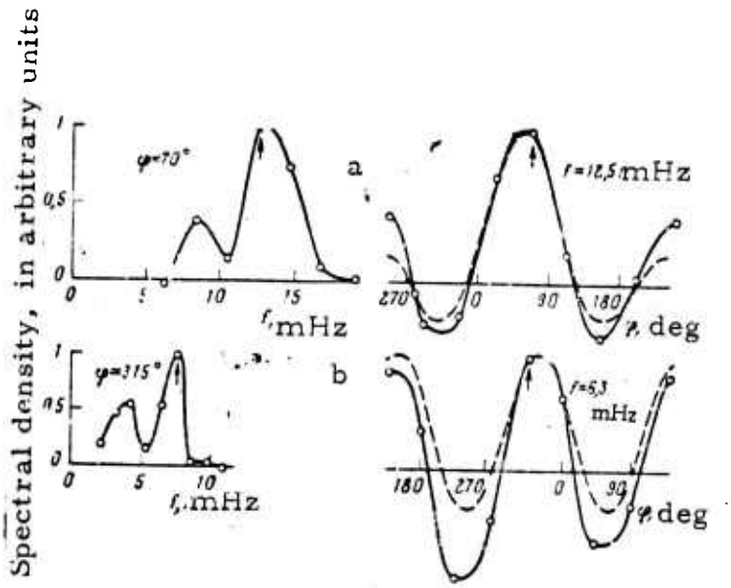

Fig. 4. Profiles of $g(\varphi, f)$ at f = const and φ = const.

Kuftarkov, Yu. M. On the theory of turbulence formation in a stratified fluid. Morskiye gidrofizicheskiye issledovaniya, no. 1, 1974, 34-43.

The onset of turbulence is described using a geostrophic model of the flow characteristics as described by a system of dynamical equations for two-point correlation moments. Expressions for the statistical parameters of turbulence, $\overline{u_3^2} = \overline{w}^2$, $\overline{u_3\theta} = \overline{w\theta}$, $\overline{\theta}^2$, are derived and treated for two cases: 1) the velocity field alone is initially disturbed; 2) the temperature field alone is initially disturbed.

1). In the case of an unstably stratified fluid with a constant mean velocity, $\overline{w}^2$, $\overline{w\theta}$, and $\overline{\theta}^2$ increase asymptotically with time if the wave number of the initial velocity fluctuations satisfies the inequality $\alpha < \sqrt[4]{\frac{g\beta\left|\frac{\partial\overline{\theta}}{\partial z}\right|}{\nu\varkappa}}$; if, however $\alpha > \sqrt[4]{\frac{g\beta\left|\frac{\partial\overline{\theta}}{\partial z}\right|}{\nu\varkappa}}$, then they decrease monotonically with time. The characteristic decay time for these functions is $\tau_1 \approx \left(\left|(\nu+\varkappa)\alpha^2 - \sqrt{(\nu-\varkappa)^2\alpha^4 - 4g\beta\frac{\partial\overline{\theta}}{\partial z}}\right|\right)^{-1}$. In the case of a stably stratified fluid,

$\overline{w}^2$, $\overline{w\theta}$, and $\overline{\theta}^2$ decrease monotonically with time if $\alpha > \sqrt[4]{\frac{4g\beta\frac{\partial T}{\partial z}}{(\nu-\varkappa)^2}}$; however when $\alpha < \sqrt[4]{\frac{4g\beta\frac{\partial T}{\partial z}}{(\nu-\varkappa)^2}}$, then $w\theta$ and θ^2 can be generated, but they decrease asymptotically with time. The characteristic decay time is then $\tau_2 \simeq \left[(\nu+\varkappa)\alpha^2\right]^{-1}$ (here ν is coefficient of kinematic viscosity, $\varkappa$ is coefficient of thermal conductivity)

2) In the case of an unstably stratified fluid, the flow is unstable if the wave number of the initial temperature fluctuations is $b < \sqrt[4]{\frac{g\beta\left|\frac{\partial T}{\partial z}\right|}{\nu\varkappa}}$; if $b > \sqrt[4]{\frac{g\beta\left|\frac{\partial T}{\partial z}\right|}{\nu\varkappa}}$ the flow is stable. In the case of a stably stratified fluid $\overline{w}^2$, $\overline{w\theta}$ $\nu\varkappa$ and $\overline{\theta}^2$ decrease monotonically when $b > \sqrt[4]{\frac{4g\beta\left|\frac{\partial T}{\partial z}\right|}{(\nu-\varkappa)^2}}$ they fluctuate and decrease with time when $b < \sqrt[4]{\frac{g\beta\left|\frac{\partial T}{\partial z}\right|}{(\nu-\varkappa)^2}}$.

A comparison of the derived expressions shows that velocity disturbances in a stratified fluid cause thermal diffusion which is equal to the energy in the vertical velocity component generated by temperature disturbances. The statistical parameters analyzed show nc dependence on Coriolis force or pressure gradients.

The author notes in conclusion that this model describes the initial turbulence if the scale of initial disturbances satisfy the inequality $l_o \leq L$, where L is the scale of mean flow.

Kuftarkov, Yu. M. On the theory of small-scale oceanic turbulence. IN: Sb. Morskiye gidrofizicheskiye issledovaniya, no. 4, Sevastopol', 1974, 49-57.

The generation mechanism for small-scale turbulence in the interior of a stratified ocean by random exterior factors is studied. The author uses a system of equations for spectral tensor functions which differs

from the Phillips system only by the addition of terms which account for viscosity and thermal conductivity. It is assumed that the level of turbulence is low. An approximate analytical solution is found in the form of an asymptotic series, for the case where the gradient of the mean temperature is small and $< 1/Re$, $Ri << 1/RePr$, $Ri << 1$. In the case of arbitrary values of Ri the system of equations for the spectral tensor functions is integrated numerically, assuming that the initial velocity disturbances represent wave motion, while temperature disturbances are absent. The article includes a discussion of Monin's hypothesis on the generation of an instability owing to the difference in coefficients of molecular heat and momentum diffusion.

The results of numerical integration show that in the case of stable stratification, at a fixed Pr number, the statistical parameters of turbulence decrease monotonically as $t \to \infty$ and small-scale motion decays. The degree of decay is determined by Re and Ri numbers. Figs. 1 and 2 illustrate the time variation of the nondimensional turbulent energy and heat flow, respectively.

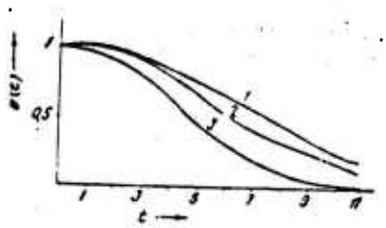

Fig. 1. Nondimensional turbulent energy at $Re = 10^4$, $Pr = 7$, $a_1 = 1$, $a_2 = 0$.

Curves 1-3: $Ri = 0.1; 0.3, 0.5$.

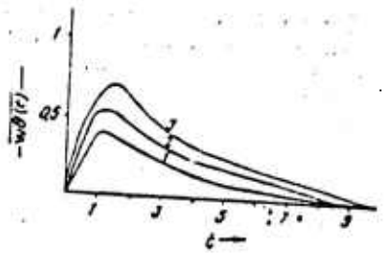

Fig. 2. Nondimensional heat flow at $Re = 10^4$, $Pr = 7$, $a_1 = 1$, $a_2 = 0$.

Curves 1-3: $Ri = 0.1; 0.3, 0.5$.

The results of numerical calculations at various values of the Pr number, which were made in order to verify Monin's hypothesis in the framework of the present model, show that within a large range of Pr numbers, the velocity disturbances decay at any values of Re or Ri > 0. Hence, in a stably stratified flow with linear profiles of mean velocity and mean temperature, any initial disturbance decays irrespective of any large differences in coefficients of heat and momentum diffusion. In the case of an unstable stratification, owing to the presence of viscosity and thermal conductivity, there exists an unstable region in the (Re, Ri) domain, as illustrated in Fig. 3. This unstable region expands as the Pr value increases.

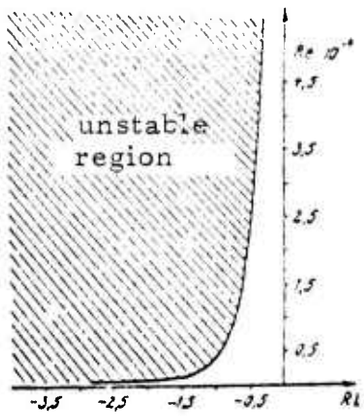

Fig. 3. Instability region in the (Re, Ri) domain at Pr = 7.

The author notes however that the system of equations for spectral tensor functions cannot be used in the study of motion within the instability region, since it does not allow for intense vertical fluxes.

Kushnir, V. M., and G. V. Smirnov. Correlation of fluctuations in horizontal flow velocity with vertical fluctuations of hydrological elements in the scale range of internal waves. Okeanologiya, no. 2, 1975, 256-260.

The object of this analysis is to compare the variance of vertical displacements in internal waves, as estimated from fluctuation

spectra of horizontal velocity, with the variance of measured vertical fluctuations of isotherms. The analysis is made using Phillips' model for small-scale internal waves at small local variations in N(z), and Fofonoff's statistical interpretation of it. The experimental data used (see Figs. 1-3) include measurements by the "Istok" probe down to 60 m, and by EPV-2 current meters set on a standard station, carried out in the Gibraltar Straits during calm weather.

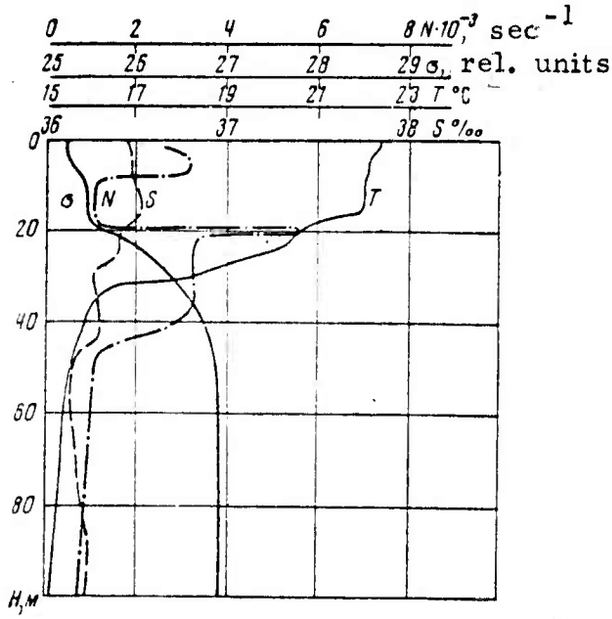

Fig. 1. Vertical profiles of σ_{STP}, S, N, and T in the Gibraltar Straits.

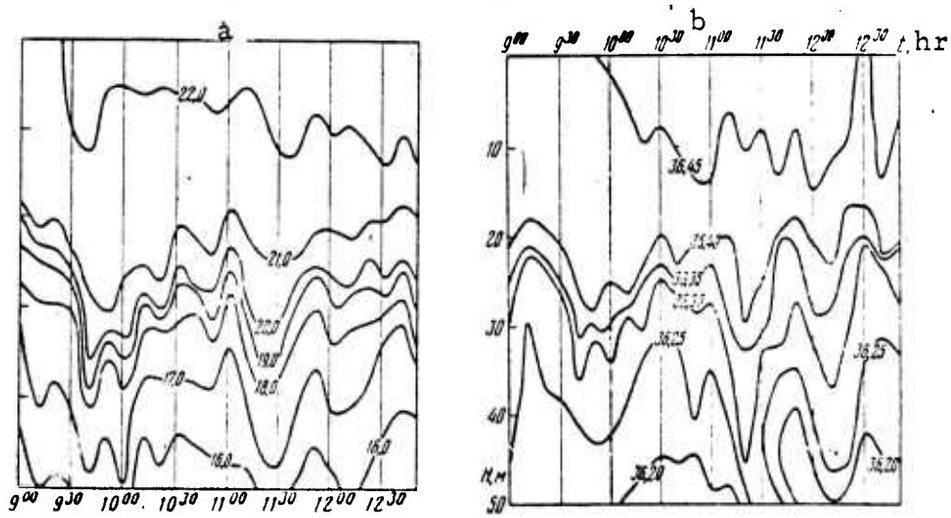

Fig. 2. Time-variations of isotherms (a) and isohalines (b) in the Gibraltar Straits.

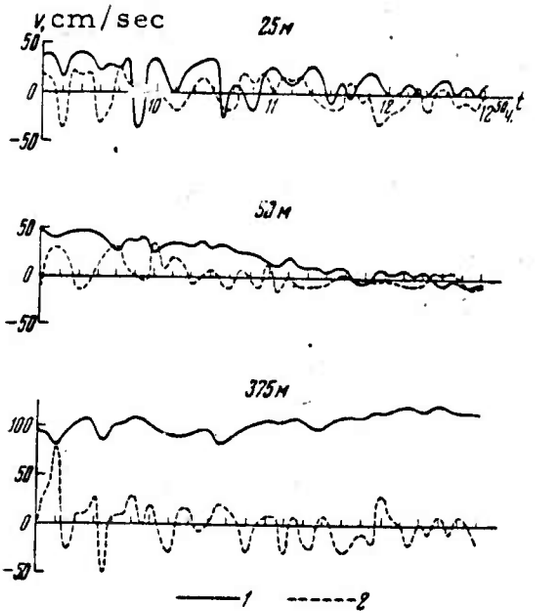

Fig. 3. Spectra of fluctuations in horizontal velocity at various depths.

The variance of vertical displacements in internal waves is calculated by

$$\sigma_{\xi q}^2 = \int_{\omega_1}^{\omega_2} \frac{S_q(\omega)\, d\omega}{N^2 - \omega^2}, \qquad (1)$$

where $S_q(\omega)$ is the spectrum of horizontal velocity fluctuations in the direction of the velocity vector. The calculated values are corrected for errors due to the distortion of $S_q(\omega)$, introduced by the discrete nature of measurements.

The experimental standard deviation σ_ξ based on the variation of isotherms, measured at 24 points at a depth of 25 m, falls into the interval $2.75\ \text{m} \leq \sigma_\xi \leq 4.55\ \text{m}$, with a probability of 0.95. The standard deviations calculated by eq. (1) with a probability of 0.95 are: $3.04\ \text{m} \leq \sigma_{\xi q} \leq 3.5\ \text{m}$ for the longitudinal velocity component; and $2.55\ \text{m} \leq \sigma_{\xi q} \leq 2.92\ \text{m}$ for the transverse component.

The agreement between the estimates for σ_ξ and $\sigma_{\xi q}$ are interpreted as in support of Phillips' model. However, the results can be applied only to internal waves at small changes in $N(z)$, i. e. between 20-40 meters depth.

Leonov, A. I., and Yu. Z. Miropol'skiy. Instability of weakly nonlinear internal gravity waves in an unbounded stratified fluid. DAN SSSR, v. 222, no. 1, 1975, 68-71.

The propagation and stability of two-dimensional nonlinear steady internal gravity waves in a weakly stratified fluid at rest are studied at $\lambda H^{-1} \ll 1$, where H is fluid depth. As the authors showed in previous works (Leonov and Miropol'skiy, 1974; 1975), in the case of two-dimensional steady internal waves in a nonviscous and nonthermoconductive fluid at rest, the hydrodynamic equations reduce to equations for the flow function only. The nondimensional form of that equation, expressed in $z=z'N_0v^{-1}$; $\vartheta=\vartheta'N_0v^{-1}$; $F=\Psi(vH)^{-1}$; and $\Omega=N^2/N_0^{-2}$ (N_0 = const is the characteristic value of the Vaisala-Brunt frequency) is given by

$$\Delta F+F\Omega(\varepsilon z-F)=\mu\left\{\varepsilon\frac{\partial F}{\partial z}-\frac{1}{2}\left[\left(\frac{\partial F}{\partial\vartheta}\right)^2+\left(\frac{\partial F}{\partial z}\right)^2\right]\right\}\Omega(\varepsilon z-F), \tag{1}$$

where

$$\varepsilon=v(HN_0)^{-1};\ \mu=HN_0^2g^{-1}.$$

At $\varepsilon\ll 1$, in the case of short waves, the problem is reduced to analysis of the propagation of internal waves in an infinitely deep fluid. It is further assumed that $\mu\leqslant\varepsilon\ll 1$ and $\mu=\mu_0\varepsilon$ where $\mu_0\sim 1$.

The solution of (1) is found by the approximate methods developed by Luke (1966) and Whitham (1970), in the form where

$$\beta=-(l^2+k^2)[2\Omega_\eta(\eta)]^{-1},\ \gamma=-3\Omega(\eta)[2\Omega_\eta(\eta)]^{-1},\ c=-3E[\Omega_\eta(\eta)]^{-1}. \tag{2}$$

Equation (2) represents either solitary or periodic waves, depending on parameters β, γ, and c.

Analysis of the solution for stationary periodic waves shows that it is stable with respect to longitudinal disturbances (along the $\zeta=\varepsilon\vartheta$ axis); but it is unstable with respect to transverse disturbances (along the $\eta=\varepsilon z$ axis). Stationary periodic waves generate a mean flow

$$\bar{U}=\frac{1}{2\pi}\int_0^{2\pi} U(\zeta)\,d\Theta\approx\frac{\Omega_\eta(\eta)}{2\Omega(\eta)}A^2+O(A^4). \tag{3}$$

Solitary waves are stable and they propagate along curvilinear paths. The amplitude of solitary waves near caustics increases without bound. Finally, in the special case where $\varphi=\varphi(\eta)$, $r=r(\eta)$ the following conservation laws apply:

$$a(\eta)\sin\varphi=\Omega^{1/4}\Omega_\eta^{-1/2}\sin\varphi=\text{const},\quad r\cos\varphi=\text{const}. \tag{4}$$

Margushina, S. G., A. A. Kharenko, A. M. Kharenko, and A. Ye. Eydel'man. Measurement of spectral characteristics of small-scale turbulence by means of a conduction anemometer. Donetsk, Donetsk University, 1975, 7 p. May 8, 1975. (RZhMekh, 8/75, #8B1055 DEP.). (Translation)

The Kolmogorov universal spectral functions are compared, as determined from measurements by hot-wire and conduction anemometers. Velocity fluctuations were measured in turbulent flow in a circular pipe.

Miropol'skiy, Yu. Z. Internal waves in the ocean generated by a wind field. Okeanologiya, no. 3, 1975, 389-396.

Generation of nonstationary internal waves with arbitrary wavelengths and N(z) by random fluctuations of a wind field is studied. Expressions for the vertical velocity spectrum of the internal waves in terms of space-time spectral density of wind friction components and their space-time cospectra are developed.

The resonant excitation of internal waves is analyzed numerically, using experimental data on the frequency spectrum of the wind velocity V (wind friction intensity is $\tau \sim V^2$). The following model of an ocean with depth H is considered: in the upper (Ekman) layer with thickness h, the density ρ_1 = const, and the eddy viscosity is a factor; below this $\rho_2 = \rho_2(z)$, and the eddy viscosity is assumed negligible.

The analysis shows that, irrespective of the modulation of vertical velocity by inertial frequency in the upper layer, the vertical velocity in the lower layer oscillates at the natural frequencies of the internal waves, with a phase shift relative to wind drag. The phase shift is determined by the ratio between the longitudinal and transverse scales of wind inhomogeneities, and by the ratio of the frequency of internal waves and inertial frequency, ω_n/f. The horizontal velocity is represented by a superposition of oscillations with frequency f and frequency ω_n. A resonant growth of the internal wave spectrum occurs only when the space-time spectral functions for the components of the wind drag contain a set of frequencies and wave numbers which correspond to the dispersion relation for free modes of internal waves.

Fig. 1 shows the growth factor for internal waves, calculated on the assumption that the oscillations of wind drag have a single mode with a period of about 10 hours, N^2 = const.

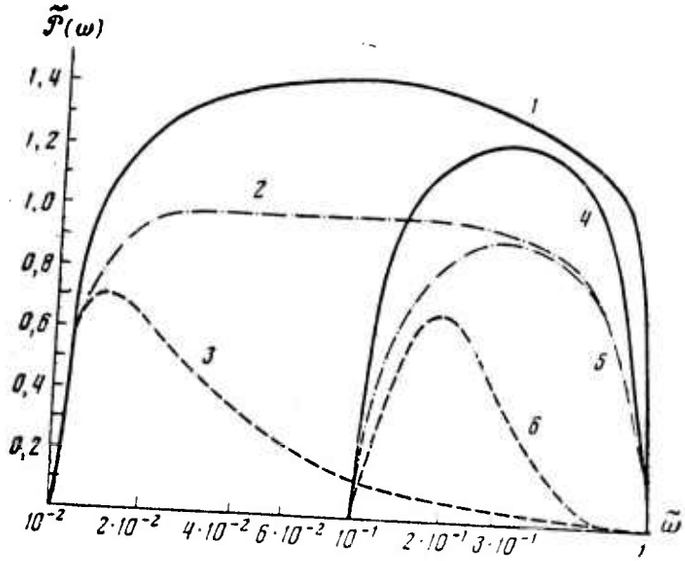

Fig. 1.

As seen in Fig. 1, the most intense generation of internal waves occurs at frequencies which are close to $\omega_* \approx N^{1/2} f^{1/2}$ and when the wind and wave directions coincide. The time for attaining the maximum amplitude of internal waves, $\epsilon_m = 10$ m at $\tilde{\eta} = n\pi\eta = \pi/2$ is estimated to be about 2.6×10^5 sec.

Netyuaylo, A. P., I. A. Sherenkov, A. I. Kobzar', V. M. Kuz'menko, and E. D. Telezhkin. Turbulent characteristics of the dynamic boundary layer of an interface between flows of different density and temperature stratification. IN: Gidravlika i gidrotekhnika. Resp. mezhved, nauch. -tekhn sb. no. 19, 1974, 8-13. (RZhMekh, 4/75, #4B1200). (Translation).

A system of equations in terms of second moments of velocity and temperature, and allowing for buoyancy forces, is analyzed. Hypotheses

proposed by Yu. Rott and B. A. Kolovandin are used for closure of the system. In the final form, after neglecting diffusion and convection terms, the system reduces to a system of algebraic equations in terms of seven second moments. In the absence of temperature stratification, these equations become Levin's formula.

Neuymin, G. G., and G. A. Tolkachenko. Experimental investigations of the space-time structure of an optical field below a wavy sea surface. Morskiye gidrofizicheskiye issledovaniya, no. 2, 1974, 55-63.

This article describes a multichannel measuring and recording system which was designed in the Marine Hydrophysical Institute, and also the measurement procedure employed in studying the space-time structure of underwater illumination. It includes an analysis of measurement errors and some preliminary results of measurements.

The measurements were performed on a stationary gradient mast in the Black Sea, 300 m offshore at a water depth of 15 meters. A general view of the gradient mast is shown in Fig. 1. Receiving units, power supply, and measuring and recording system were installed onshore. Hermetically-sealed selenium photocells are used as photodetectors. Their working surface is 3 cm^2, sensitivity = 430 $\pm$ 15 μa/ln, and the frequency range = 60-520 nm. A plane collector, placed in the front of a light filter, has a receiving surface with a diameter of 36 mm. Measurements at ten levels (see Fig. 2) were made in the form of a series 2-3 minutes long. The maximum overall measurement error was found to be 5%.

The results of calculations are shown in Figs. 2-4.

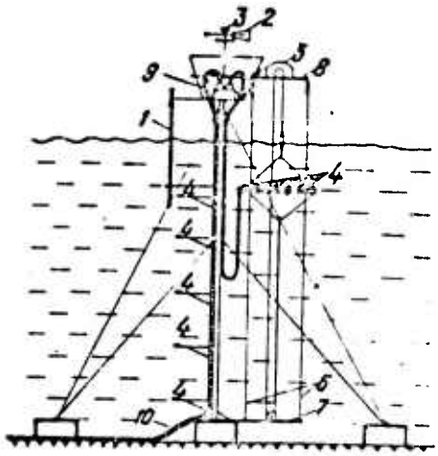

Fig. 1. Instrumentation of gradient mast.

1- wavegraph with coaxial capacitance-type sensor; 2, 3- sensors of wind velocity and direction; 4- luminance sensors; 5- winch; 6- guide wire; 7, 8- extendable booms; 9- connectors; 10- cable to onshore lab.

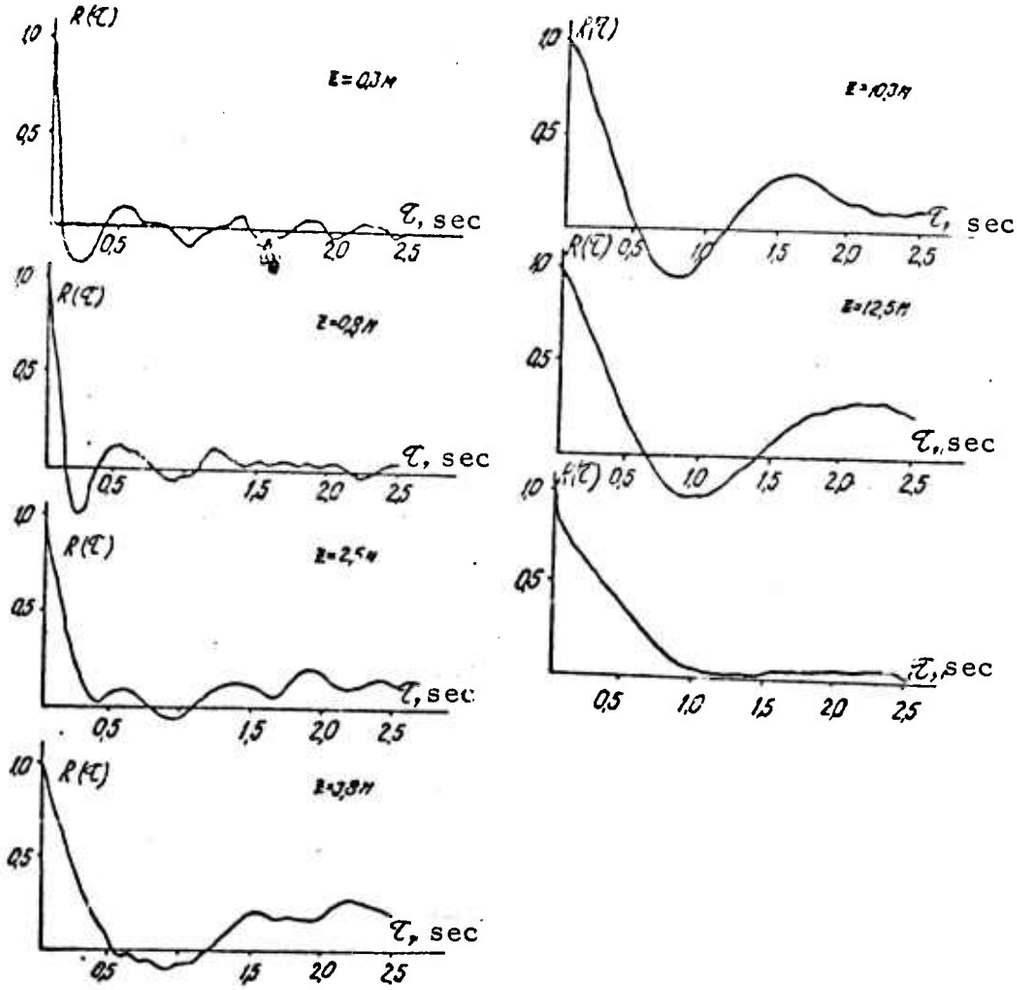

Fig. 2. Normalized autocorrelation functions for fluctuations of underwater illuminance at depths of 0.3, 0.8, 2.5, 3.8, 10.3, and 12.5 m, and normalized autocorrelation function for fluctuations of elevation of the surface (lowermost curve).

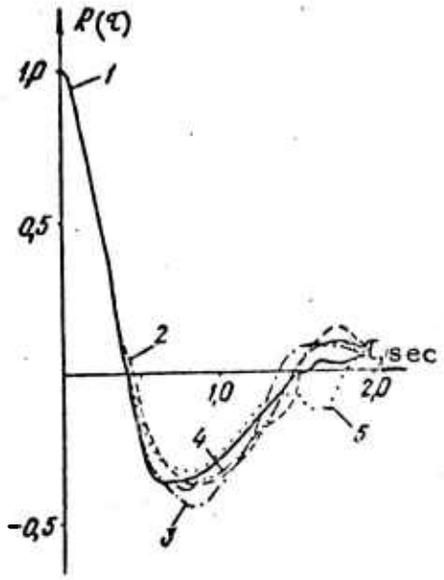

Fig. 3. Normalized autocorrelation fluctuations of underwater illuminance at a depth of 1.5 m. Sensors spaced by 20, 40, 60, and 80 cm. Numerals indicate sensors.

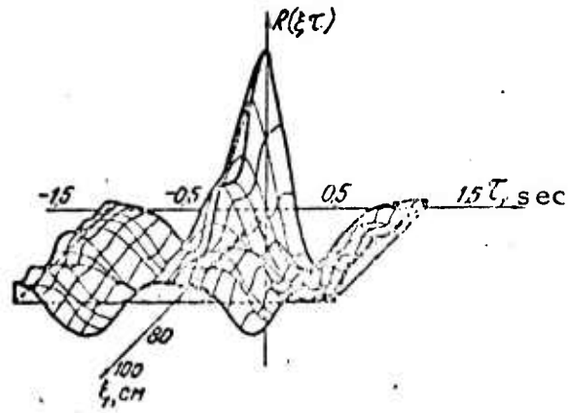

Fig. 4. Space-time correlation function for underwater illuminance field measured at a depth of 1.5 m. 10 cm-spaced sensors located in N-S direction.

Nikishov, V. I. On applying the method of perturbations to the theory of internal waves. IN: Gidromekhanika. Resp. mezhved. sb., no. 30, 1974, 59-63. (RZhMekh, 5/75, #5B539). (Translation)

The method of perturbations is applied to establish the possible modes and horizontal wave numbers of small oscillations in a density-stratified ocean with finite depth. Application limits for this method are determined.

Osipov, Yu. S., N. I. Zhidkova, and L. D. Pukhtyar. Methods of calculating three-dimensional turbulent diffusion in the sea. Trudy Gosudarstvennogo okeanograficheskogo instituta, no. 125, 1975, 59-65. (RZhMekh, 8/75, #8B609). (Translation)

A method for calculating vertical and horizontal turbulent diffusion of a tracer in the ocean is considered. Vertical diffusion can be calculated using existing solutions of the semiempirical equation of turbulent diffusion. The calculation of horizontal diffusion is based on the statistical theory of turbulent diffusion. A formula is given for the calculation of the parameters of horizontal diffusion. Data on Lagrangian turbulence obtained in experiments with freely - drifting floats are given.

Panchev, S. Existence of power relationships in spectra of oceanic turbulence. FAiO, no. 6, 1975, 620-625.

The behavior of oceanic turbulence spectra in the buoyancy interval is investigated, by use of similarity theory and dimensional arguments. The following assumptions are made: a) the turbulence is stationary in the sense that its statistical parameters are time-independent over sufficiently long intervals; b) the turbulence is horizontally homogeneous, while the gradients of U(z) and $\bar{\rho}(z)$ are constant within a given layer; c) the density fluctuations are induced mainly by temperature fluctuations, i.e. $\rho' \sim \alpha_0 \bar{\rho} T'$, where $\alpha_0 = 2 \times 10^{-4}$ deg^{-1} is the coefficient of thermal expansion for water; d) the effect of molecular viscosity and diffusion may be neglected. Introducing $\beta = \alpha_0 g$, $\gamma = \partial \bar{T}/\partial z$, $b = \partial U/\partial z$, the following dimensional parameters then determine the turbulence spectra: γ [deg/cm], b [sec^{-1}], β [cm/sec^2 deg], ϵ [cm^2/sec^3], and ϵ_T [deg^2 sec] where ϵ and ϵ_T are energy dissipation rates for velocity and temperature fluctuations.

Using for the generalized scale

$$L = \varepsilon^{x_1} \varepsilon_T^{x_2} b^{x_3} \gamma^{x_4} \beta^{x_5}. \tag{1}$$

and expressing x_1, x_4, and x_5 through x_2 and x_3, Eq. (1) becomes

$$L = \varepsilon^{1/3} / (\beta\gamma)^{3/4} (\varepsilon_T \beta / \varepsilon\gamma)^{x_2} (b / \sqrt{\beta\gamma})^{x_3}; \tag{2}$$

by introducing ϵ_T^*, eq. (2) becomes

$$L = \varepsilon^{1/3} N^{-3/2} f_1 (b / N) f_2 (\varepsilon_T^* / \varepsilon), \tag{3}$$

where $f_1(x)$ and $f_2(y)$ are nondimensioral functions and ϵ_T^* is the formal mechanical equivalent of ϵ_T.

The particular cases of (2) are

a)	$x_2 = x_3 = 0$,	$L_1 = L_0 = \varepsilon^{1/3} N^{-3/2}$,
b)	$x_2 = -3/4$, $x_3 = 0$;	$L_2 = L_* = \varepsilon^{3/4} \beta^{-3/2}$,
c)	$x_2 = 3/4$, $x_3 = 0$;	$L_3 = L_T = \varepsilon_T^{3/4} \varepsilon^{-1/4} \gamma^{-3/2}$,
d)	$x_2 = 1/2$, $x_3 = 0$;	$L_4 = L_T^* = \varepsilon_T^{*1/2} N^{-3/2}$,
e)	$x_2 = 0$, $x_3 = -3/2$;	$L_5 = L_u = \varepsilon^{1/3} b^{-3/2}$,
f)	$x_2 = 1/2$, $x_3 = -5/2$;	$L_6 = \varepsilon_T^{1/2} \beta b^{-3/2}$,
g)	$x_2 = 1/2$, $x_3 = -1/2$;	$L_7 = \varepsilon_T^{1/2} \gamma^{-1} b^{-1/2}$.

(4)

It is shown that length scales L_o and L_u can be given a physical interpretation.

In order to analyze the effects of stratification on spectra, eq. (3) is rewritten in a simplified form for b = 0:

$$L = \varepsilon^{1/3} N^{-3/2} f_2 (\varepsilon_T^* / \varepsilon). \tag{5}$$

At $k << k_o = (\epsilon/\nu)^{1/3}$, the turbulent spectra are given in the form (Monin and Yaglom, 1967):

$$\Phi(k) \sim \varepsilon^{2/3} k^{-5/3} \varphi(kL), \quad \Phi_T(k) \sim \varepsilon_T \varepsilon^{-1/3} k^{-5/3} \varphi_T(kL), \quad \Phi_{WT}(k) \sim \varepsilon_T^{1/2} \varepsilon^{1/6} k^{-5/3} \varphi_{WT}(kL), \tag{6}$$

where L is given by eq. (5).

Functions φ_i (kL) in eq. (6) are determined theoretically, assuming that: a) at $kL << 1$, ϵ is negligible; b) the stratification effect in eq. (6) is initiated at the same minimum scale of (5). It then follows that $f_2(x) \sim x^n$, $\varphi(y) \sim y^m$, $\varphi_T(y) \sim y^p$, $\varphi_{WT}(y) \sim y^q$. Substituting these expression into eq. (6) and introducing the quantity $\delta = 4/3\,(1-2n)$, the spectra are given by

$$\Phi(k) \sim \varepsilon_T^{*1/2} N^{-1/2} (kL_T^*)^{-\frac{5}{3}-\delta}, \quad \Phi_T(k) \sim \varepsilon_T \varepsilon_T^{*1/2} N^{-1/2} (kL_T^*)^{-\frac{5}{3}-\frac{\delta}{2}},$$
$$\Phi_{W_T}(k) \sim \varepsilon_T^{1/2} \varepsilon_T^* N^{-1/2} (kL_T^*)^{-\frac{5}{3}-\frac{\delta}{4}}, \tag{7}$$

where $\delta \geq 0$ is an arbitrary constant and L_T^* appears automatically.

Eqs. (7) indicate that in the buoyancy interval, various slopes and levels of spectra are possible. This conclusion agrees with experimental data.

The article also contains numerical estimates of eq. (4), discussion of eq. (6) at $\delta = 0$, and discussion of the parameter ϵ_T^*/ϵ, which is shown to be a measure of the stability of the medium.

The author points out that the present analysis does not answer questions of conditions for existence of spectra (7) in the buoyancy interval, nor of determination of φ_i (kL) at $kL \approx 1$.

Pivovarov, A. A., and G. S. Mukoseyeva.
Temperature waves in the sea for the case of extended heat sources and variable intensity of turbulent heat exchange. VMU, no. 3, 1975, 374-376.

Stationary temperature fluctuations (deviations from daily mean) are analyzed for the case of the following model of depth variation in the coefficient of turbulent heat exchange:

$$k(z) = \begin{cases} k_0 + az & 0 \leq z \leq h \\ (k_0 + ah)\, e^{-c(z-h)} = be^{-c(z-h)} & h \leq z < \infty \end{cases}. \tag{1}$$

The distribution of temperature fluctuations t_j is defined by

$$\frac{\partial t_j}{\partial \tau} = \frac{\partial}{\partial z} k_j(z) \frac{\partial t_j}{\partial z} + \frac{Q_0(\tau)}{c_1 \rho} \sum_{m=1}^{\nu} I_m \beta_m e^{-\beta_m z}; \quad j = 1, 2 \tag{2}$$

and the boundary conditions by

$$\begin{gathered} z = 0 \quad t_1 = f(\tau); \quad z \to \infty \quad t_2 = 0; \\ z = h \quad t_1 = t_2; \quad \frac{\partial t_1}{\partial z} = \frac{\partial t_2}{\partial z}. \end{gathered} \tag{3}$$

where C_1, ρ are specific heat and density for seawater, I_m and β_m are the fraction and internal attenuation respectively for the m-th section of the spectrum of summary flux of radiant energy, $Q_o(\tau)$, which penetrates the water.

A general solution is found in the form of a series,

$$t_j(z, \tau) = \mathrm{Re} \sum_{n=1}^{\infty} \theta_{jn}(z)\, e^{-in\omega\tau}. \tag{4}$$

The results of the analysis show that the effect of internal absorption of radiant energy on temperature fluctuations in the sea is closely correlated with the nature of the depth-variation of turbulent heat exchange. Calculations of amplitude and phase shift for the first harmonic of temperature waves, using k(z) as observed in the Black Sea (Voskanyan, 1970) are presented graphically.

Polyanskaya, V. A., and Ye. G. Kharat'yan. Acoustic field in the ocean in the presence of high-frequency internal waves. Akusticheskiy zhurnal, no. 3, 1975, 436-447.

An evaluation is given of the distortion by internal waves of the acoustic field in the gradient layer. A simple model of the gradient layer, which is disturbed by primary-mode internal waves, is considered in the framework of ray geometry. Numerical calculations are made for the acoustic field at distances up to the second convergence zone, using experimental data on hydrological parameters (see Fig. 1). Results are

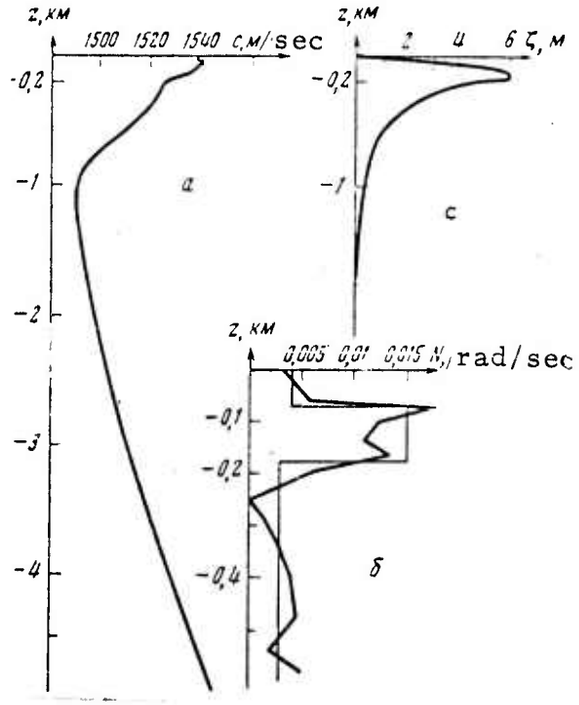

Fig. 1. Vertical profiles of sound velocity (a), Vaisala frequency (b), and vertical displacement in internal waves (c).

compared to earlier findings by Polyanskaya (1974). The analysis is made for the distribution of refractive index n, defined by

$$n^2(x,z)=\begin{cases}1, & z\geqslant\zeta,\\ 1-\gamma(z-\zeta), & -h+\zeta\leqslant z<\zeta,\\ 1+\gamma h=n_1^2, & z<-h+\zeta,\quad \gamma\gtrless 0.\end{cases} \tag{1}$$

where z is directed upwards; ξ (x, z) describes the distribution of vertical displacements in the internal waves with wavefronts parallel to y. Within the gradient layer $\xi(x) = a\cos(kx + \mu)$, where a, k, μ are amplitude, wave number, and phase of primary-mode internal waves, respectively.

The analysis shows that the presence of a train of internal waves in the gradient layer affects the acoustic ray pattern in the following manner: 1) slip angles change for rays which traverse, or are bent in, the gradient layer (see Fig. 2); the change, which depends on phase of internal waves, for rays which traverse the layer is given by

$$\beta_{cn}^2-2|\gamma|a\leqslant\beta_1^2\leqslant\beta_{cn}^2+2|\gamma|a,\quad \beta_{cn}^2=\beta_0^2+\gamma h. \tag{2}$$

while for rays which are bent,

$$\beta_0^2-2|\gamma|a\leqslant\beta_{01}^2\leqslant\beta_0^2+2|\gamma|a. \tag{3}$$

2) Additional caustic surfaces occur. Return lines for these caustics are localized in the near illuminated zone, or only in the convergence zones, depending on the thickness of the gradient layer and the amplitude of the internal waves. The distortion due to internal waves can be roughly evaluated with a formula for the minimum depth of the return line in the homogeneous half-space beneath the gradient layer:

$$z_1-z_0\sim\beta^3/(\gamma ak\cos\alpha_0)\approx\sqrt{2\Delta c/c}\cdot h/(ak\cos\alpha_0). \tag{4}$$

3). The change in slip angles can lead to the appearance of new congruences, such as congruences III and IV in Figs. 3-5.

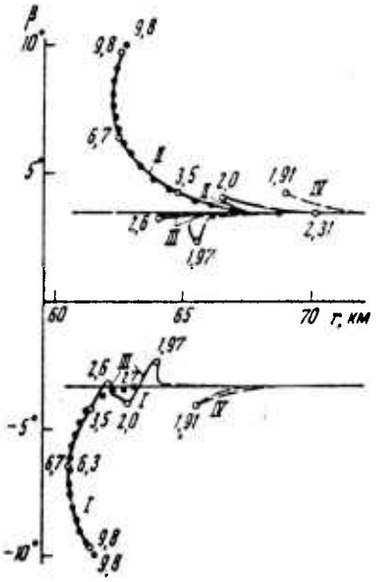

Fig. 2. Slip angles of rays refracted at internal waves at 100 m depth.

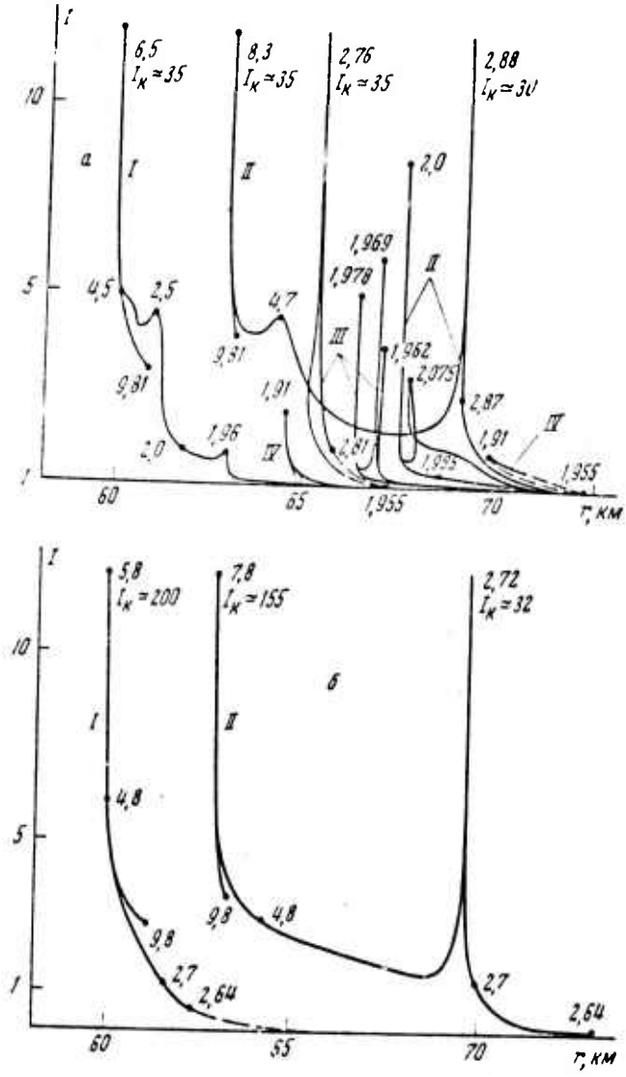

Fig. 3. Relative amplitude of acoustic field at a depth of 200 m in the first zone of convergence.

a - internal waves present; b - absent.

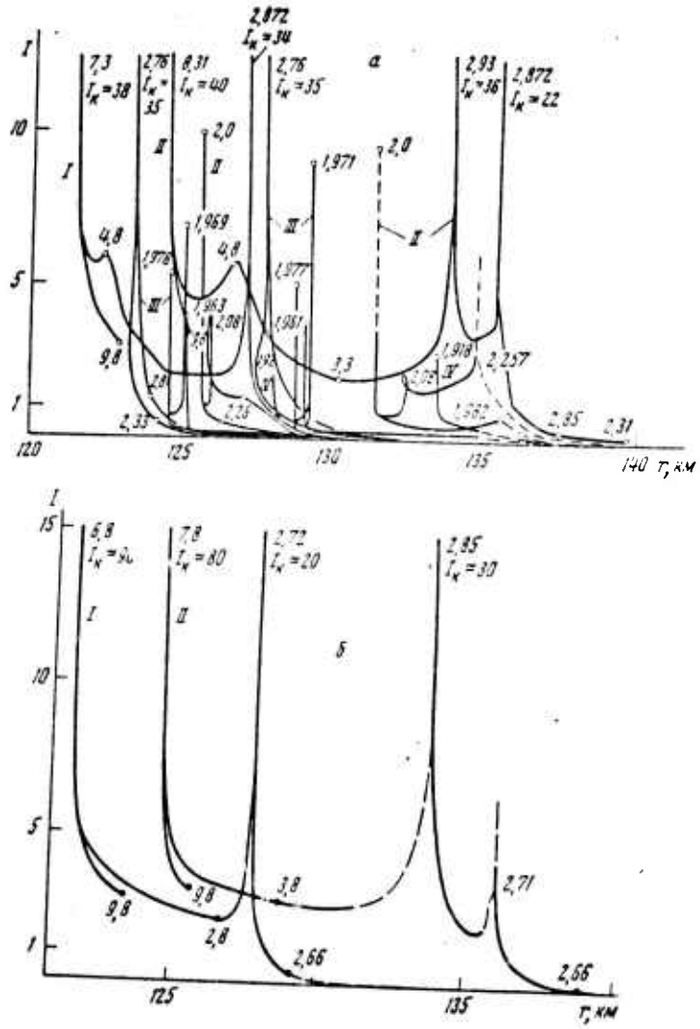

Fig. 4. Relative amplitude of acoustic field at a depth of 200 m in the second zone of convergence.

a- internal waves present; b- absent.

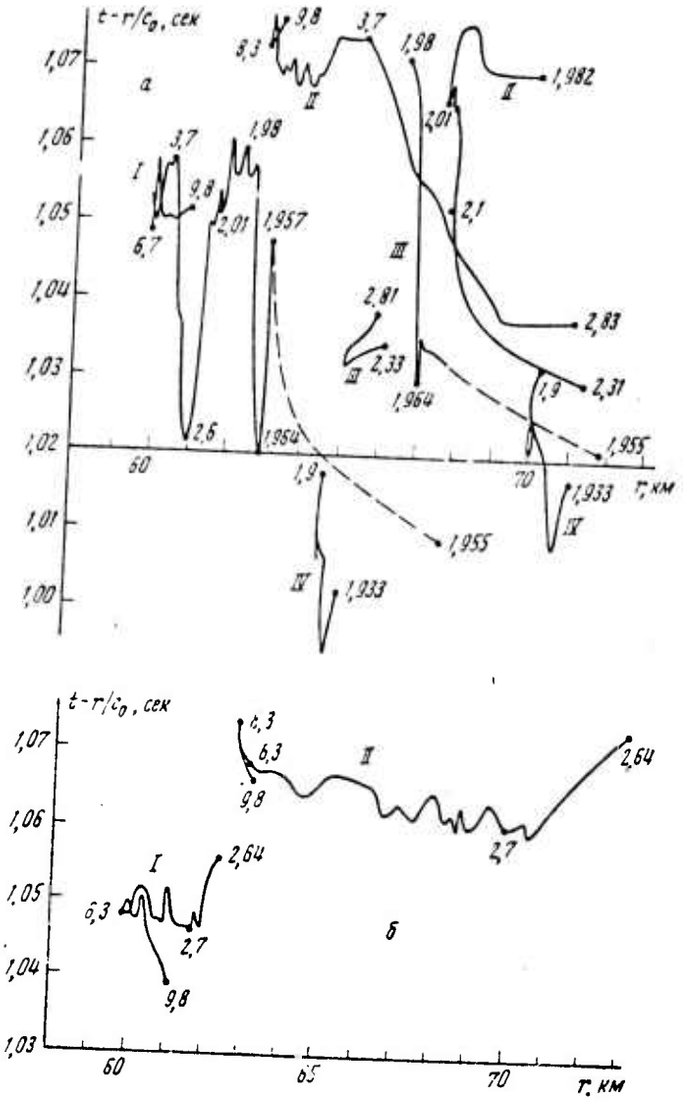

Fig. 5. Arrival times $t - r/C_o$ ($C_o = C(0, -H)$ for acoustic pulses at a depth of 200 m in the first zone of convergence.

a- internal waves present; b- absent.

Prokhod'ko, V. P. Computation of averaged velocity and pulsating energy in a turbulent axisymmetric wake far behind a streamlined body. IN: Gidromekhanika. Resp. mezhv. sb. No. 29, 1974, 13-18. (RZh Vodnyy transport, 5/75, #5A58). (Translation)

The results are given of calculations for a turbulent axisymmetric wake far astern of a towed, streamlined body by use of the equation for turbulent energy balance. Several semiempirical approximation schemes are considered. The results of computations agree satisfactorily with experimental data.

Resnyanskiy, Yu. D. Parametrization of integral dissipation of turbulent energy in the upper quasi-homogeneous ocean layer. FAiO, no. 7, 1975, 726-733.

The possibility is considered of using similarity theory for the parametrization of integral turbulent energy dissipation D in the upper quasihomogeneous oceanic layer. A general expression for D, as well as approximations for some special cases, is obtained. The effect of nonstationary factors in the thermal structure of the upper ocean layer is analyzed for periods of warming and cooling of the ocean. The author hypothesizes that, in order to describe the nonstationary turbulent regime in the upper quasi-homogeneous ocean layer, it is sufficient to introduce only one additional parameter, namely the thickness h, to those used in the similarity theory. Similarity theory for the horizontal, homogeneous boundary layer of the atmosphere is defined by Kazanskiy and Monin (1960). The expression for the integral turbulent energy dissipation that follows from dimensional arguments is then

$$D/\rho = v_*^3 D_n (h/L_1, N), \qquad (1)$$

where $L_1 = v_*/\Omega$, $N = L/L_1$ is the Kazanskiy-Monin dimensionless stratification parameter; $L = v_*^3/(g \alpha Q_o/\rho c_p$ is the Monin-Obukhov length

scale; D_n is a dimensionless function of the two arguments, $v_* = (\tau_o/\rho)^{1/2}$, τ_o is tangential turbulent stress in the near-surface layer, Q_o is turbulent thermal flux at the ocean surface, and ρ and c_p are density and specific heat for water. The function D_n is determined indirectly for different models of the upper quasihomogeneous layer.

Timchenko, I. Ye., and V. D. Yarin.
Sequential analysis of observations on vertical temperature distribution in the Gulf of Lyon.
Morskiye gidrofizicheskiye issledovaniya, no. 3, 1973, 116-129.

An attempt is made to apply the method of sequential analysis (Kalman, 1960; Petersen, 1970) to oceanographic data. Temperature observations were made at depths of 0, 5, 10, 15, 20, 30, and 60 m at the French buoy laboratory in the Gulf of Lyon, under conditions of calm seas during the joint Franco-Soviet expeditions in 1969. The vertical temperature distribution was modeled by neglecting advection, horizontal turbulent exchange, and inertial oscillations of the flow velocity field. The article contains an analysis of the convergence of the iterative algorithm of filtering, and an estimate of the applicability of the simplified model of the temperature field.

The results indicate that 1 to 4 hour forecasting of vertical temperature distribution in the sea can be achieved with tolerable accuracy.

Vishnyakov, A. A. On a model of a turbulent boundary layer as the source of a pressure pulsation field on a surface in the flow. IN: Gidromekhanika. Resp. mezhved sb., 1974, no. 30, 14-22. (RZhMekh, 5/75, #5B1121). (Translation)

An eddy model of a turbulent boundary layer is considered and its nondimensional parameters are given, which makes it possible to compute the space-time energy spectrum of turbulent fluctuations in pressure at a surface within a flow.

Vishnyakov, A. A. Discrete nature of turbulence spectra of pulsed pressures. IN: Gidromekhanika. Resp. mezhved. sb., 1974, no. 30, 22-27. (RZhMekh, 5/75, #5B1122). (Translation)

The possible causes are discussed for multiple-peak energy spectra of pressure fluctuations on a surface within a flow in a turbulent boundary layer.

The first All-Union symposium on the study of small-scale oceanic turbulence. Okeanologiya, no. 3, 1975, 552-553.

This symposium was held from September 24-27, 1974 in the city of Kaliningrad. Fifty papers were presented which discussed the following problems:

1) generation and properties of small-scale turbulence;
2) apparatus and methods used;
3) automation of data collection and processing;
4) calibration service in hydrophysical research.

The symposium demonstrated that considerable success was attained during the last 2-3 years. The Institute of Oceanology im. P. P. Shirshov has developed towed and dipped systems for measuring fluctuations of hydrophysical fields and background hydrometeorological parameters in the ocean. The Marine Hydrophysical Institute has developed self-contained deep-water measuring systems working over wide frequency ranges. Measuring systems based on optical methods have been developed by the All-Union Scientific Research Institute for Physical and Radiotechnical Measurements, and the Institute of Automation and Telemetry of the Academy's Siberian Branch. Measuring techniques based on ferroelectric ceramics have been developed by the Moscow Institute of Engineering and Physics. The first recoverable free-diving drone instrumented with hydrophysical sensors was developed jointly by the Kazan Aviation Institute and the Institute of Oceanology.

Measurements of turbulence were carried out in various characteristic regions of the World Ocean. Joint cruises of the R/V's Dmitriy Mendeleyev and Akademik Vernadskiy in the Indian Ocean during 1972 were especially successful; the analysis of measurements made resulted in construction of the first models of small-scale oceanic turbulence.

Among shortcomings in research, the following problems were stressed: decentralization of efforts, lack of participation of leading facilities in the development of fine-scale measuring instruments and systems; poor instrument standards support; lack of standards and calibrating devices; and deficiencies in equipping research vessels with specialized computers.

The symposium set the following tasks: a) improving of hydrophysical field transducers using optical and acoustical measuring methods; b) creating standard [calibrating] apparatus, test benches, and calibrating services; c) creating new types of instrument platforms for measuring

apparatus with higher noise rejection, as well as new onboard equipment for deep-sea measurements (up to 5-6 km); d) using existing systems for data recording, storage, and processing; e) extending research during expeditions to study actual mechanisms of generation and attenuation of turbulence in the ocean and their relationship to general hydrometeorological conditions; f) intensifying theoretical studies on hydrodynamic models of oceanic turbulence on the basis of experimental data collected.

The symposium requested the establishment of a Section for Oceanic Turbulence within the Oceanographic Commission of the Presidium of the Academy of Sciences.

2. Surface Effects

Andreyev, B. M. Methods of measuring sea waves by means of a shortwave radar. IN: Sb. Nekontaktnyye metody izmereniya okeanograficheskikh parametrov. Moskva, Gidrometeoizdat, 1975, 83-90. (R ZhGeofiz, 9/75, #9V42). (Translation)

A method attributed to S. Zubkovich for determining heights of wind waves, based on the ratio between coherent and noncoherent components of a signal reflected by a disturbed sea surface, is described. This method has been tested in the Caspian Sea, Gulf of Finland and Lake Ladoga. An analysis of the envelope of the fluctuating signal is performed, and a relationship between frequency spectra for waves determined from nonradar and radar data is obtained in the framework of linear theory. Special attention is given to the possible use of this method for observations aboard satellites. In that case, a large part of the ice-free ocean surface would be accessible to observations.

Babayev, A. B., Ye. V. Bogomolova, V. P. Prakhov, Yu. A. Petrov, A. M. Nedelyayev, and V. S. Fomin. Effect of polarization on statistical characteristics of a signal reflected from the sea surface in the uhf range. IN: Sb. Prikladnyye zadachi rasseyaniya i difraktsii radiolokatsionnykh signalov. Leningrad, 1974, 13-16. (RZhF, 3/75, #3Zh130). (Translation)

Results are given of an experimental study on the dependence of specific effective [sea surface] scattering area, and backscatter pattern, on the polarization of transmitted and received signals. Studies were carried out at 7 and 15 cm wavelengths.

Babayev, A. B., Ye. V. Bogomolova, G. P. Grudinskaya, V. P. Prakhov, V. S. Fomin, G. P. Shelomanova, and Yu. A. Petrov. Investigation of the angular dependence of the unit effective scattering area of a sea surface in the uhf range. IN: Sb. Prikladnyye zadachi rasseyaniya i difraktsii radiolokatsionnykh signalov. Leningrad, 1974, 23-28. (RZhF, 3/75, #3Zh132). (Translation)

Experimental studies are described on reflective properties of the sea surface. The effect of radiation angle and wind velocity on the shape of the backscatter pattern, as well as on the specific effective scattering area, are analyzed.

Babayev, A. B., V. P. Prakhov, and Yu. A. Petrov. Determination of slope spectra of a wavy surface from reflected signal characteristics in the uhf range. IN: Sb. Nekontaktnyye metody izmereniya okeanograficheskikh parametrov. Moskva, Gidrometeoizdat, 1975, 97-103. (RZhGeofiz, 9/75, #9V44). (Translation)

Measurements of [sea wave] slope spectra can be made if the dimensions of the irradiated area do not exceed the linear dimensions of large waves. When the slope of the irradiated area changes, the incident angle of r-f waves changes, causing a change in the intensity of the reflected signal detected by the receiver. The case of vertical irradiation of a disturbed sea surface is considered. The dependence of receiver output signal level, as a function of time, on the slope of the disturbed surface is obtained under some simplifying assumptions.

Babayev, A. V., V. P. Prakhov, and Yu. A. Petrov. Determination of the mean period of a sea wave from its reflected signal characteristics in the uhf range. IN: Sb. Nekontaktnyye metody izmereniya okeanograficheskikh parametrov. Moskva, Gidrometeoizdat, 1975, 111-114. (RZhGeofiz, 8/75, #8V35). (Translation)

Wavegrams obtained simultaneously by wire wave gages at the State Institute of Oceanography and by radar were processed on a Minsk-22 computer in order to calculate spectra. Recordings were made by means of a rotating-mirror oscillograph. The following conclusions are drawn: 1) peak frequencies of spectral densities determined by contact and remote methods coincide; 2) peak frequency, which is proportional to mean wave period, is practically constant for all radiation angles, from vertical to grazing; 3) the difference between mean periods as determined by the two methods was less than 7.5% for all sea conditions existing during measurements, i.e. sea states from 1 to 6; 4) as the radiation angle changes from vertical to grazing, the spectrum of the output signal becomes narrower. The latter fact confirms the conclusion that slope spectra determined by the remote method will narrow when the irradiated area is enlarged, for a given radar beam width.

Belousov, P. S., A. A. Zagorodnikov, V. I. Korniyenko, V. S. Loshilov, and K. B. Chelyshev. Results from wave measurements by radars with high area resolution in the "Bering" experiment. IN: Sb. Nekontaktnyye metody izmereniya okeanograficheskikh parametrov. Moskva, Gidrometeoizdat, 1975, 34-41. (RZhGeofiz, 9/75, #9V36). (Translation)

Two questions are considered in sea surface radar experiments: 1) to determine whether the spectrum of the radar image of a wavy surface,

obtained by side-look radar, is invariant with respect to direction of radiation; 2) to clarify the effect of foam strips on the spectrum of the radar image. Airborne measurements to check these factors were carried out in the Bering Sea at flight altitudes of 3000 m. The answers to both questions are positive [sic] .

Garnaker'yan, A. A., and A. A. Sosunov. Relation of phase fluctuations in r-f signals reflected from a sea surface to height of the waves. IN: Sb. Nekontaktnyye metody izmereniya okeanograficheskikh parametrov. Moskva, Gidrometeoizdat, 1975, 55-58. (RZhGeofiz, 9/75, #9V39) (Translation)

The standard deviation in the phase of a [sea surface] reflected signal is functionally related to some parameter which is proportional to dispersion in slopes of the disturbed sea surface. For the entire range of heights of wind waves the dispersion can be determined by varying transmitter frequency, or by using two fixed transmitter frequencies. The method can be realized by means of a coherent meter-band radar.

Garnaker'yan, A. A., A. A. Sosunov, V. T. Lobach, A. A. Timokhin, and K. L. Afanas'yev. The problem of measuring the height of sea waves by radar. IN: Sb. Nekontaktnyye metody izmereniya okeanograficheskikh parametrov. Moskva, Gidrometeoizdat, 1975, 59-66. (RZhGeofiz, 9/75, #9V40). (Translation)

A theory of measuring wave heights by shortwave vertical irradiation of a disturbed sea surface is described. Variance of wave

ordinates is functionally related to the ratio between energies of incoherent and coherent components of the reflected signal. This ratio is defined by mean value and standard deviation of fluctuations in the reflected signal envelope. To measure wave heights over an adequate range requires a 10-60 meter band radar capability. A block-diagram of a radar used for such measurements is given.

Kireyev, I. V., and A. V. Svechnikov.
Phenomenon of coherent reflection of pulsed radiosignals from a wavy sea surface.
Meteorologiya i gidrologiya, no. 6, 1975, 97-100.

A simple model of radiowave reflection from a wavy sea surface is considered. It explains the absence of a dependence of the average envelope frequency of the reflected signal on the relative speed of the radar antenna (a phenomenon observed during measurements of sea waves by shipborne navigation radar). The results of the analysis are compared to experimental data obtained in the Caspian Sea, and Atlantic and Pacific Oceans.

A simplified section of an ocean wave irradiated by a 3 cm radar is shown in Fig. 1. Phase and amplitude modulation of the reflected signal

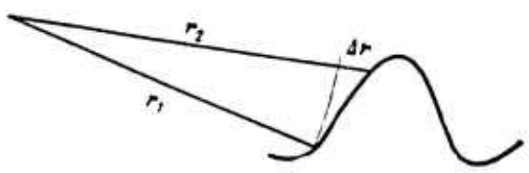

Fig. 1. Wave irradiation model.

is considered, taking into account only the orbital particle motion in sea waves. The phase of the signals reflected from the two sections of the radiated area (see Fig. 1) are

$$\varphi_1 = 2\frac{2\pi}{\lambda}(r_1 + V_A t - V_1 t) + \psi_1 + \psi_0, \quad (1)$$

$$\varphi_2 = 2\frac{2\pi}{\lambda}[r_1 + V_A t + \Delta r - (V_1 + \Delta V)t] + \psi_1 + \psi_0, \quad (2)$$

where ψ_1 - phase change during reflection;

ψ_o - initial phase

V_1 - projection of the velocity of orbital particle motion onto the direction of radiation in the first section of the radiated area;

V_A - projection of the antenna speed onto the direction of radiation;

ΔV - difference between projections of orbital velocity in the two sections of the radiated area;

The phase difference for the two signals is then given by

$$\varphi_2 - \varphi_1 = 2\,\frac{2\pi}{\lambda}\,(\Delta r - \Delta V t). \tag{3}$$

The phase difference φ_2 - φ_1 is independent of r_1, r_2 or initial phase. Thus forward motion and roll of the ship do not affect the phase difference of the reflected signals.

The field amplitude for the two interfering sinusoidal signals is given by

$$E(t) = \sqrt{E_1^2 + E_2^2 + 2E_1E_2\cos(\varphi_2 - \varphi_1)}. \tag{4}$$

If it is assumed that $E_1 = E_2$,

$$E(t) = 2E_1\cos\left(\frac{2\pi}{\lambda}\Delta r - \frac{2\pi}{\lambda}\Delta V t\right). \tag{5}$$

After corresponding substitution for ΔV,

$$E(t) = 2E\cos\left[\frac{2\pi}{\lambda}\Delta r + 2\,\frac{2\pi}{\lambda}\,V_{op}\,t\sin\frac{\beta}{2}\sin\left(\omega_M t + \frac{\beta}{2}\right)\right] = 2E\cos\left[\varphi_0 + \varphi(t)\right]. \tag{6}$$

In radar measurements of sea waves, the wave height is determined from the average frequency of the envelope of the reflected signal, F_{av}. If

$$\Omega(t) = \frac{d\varphi(t)}{dt}, \quad \Omega_{av} = \frac{2}{T}\int_0^{\frac{T}{2}} \Omega(t)\,dt, \tag{7}$$

then

$$2\pi F_{av} = \Omega_{av} = 2\pi\,\frac{2V_{or}}{\lambda}\sin^2\frac{\beta}{2}. \tag{8}$$

The calculations of F_{av} from radar data obtained in the Caspian Sea, Atlantic Ocean, and Pacific Ocean are given in Table 1, column 2. Corresponding experimental values from simultaneous observations by a GM-62 wavegraph are given in columns 3 and 4.

Table 1

1	2	3	4	1	2	3	4
No. of wave-gram	F_{av}, Hz	$F_{15\%}$, Hz	F_{av}, Hz	No. of wave-gram	F_{av}, Hz	$F_{15\%}$, Hz	F_{av}, Hz
2	77,5	90	61	13	69,5	131	68
3	65	131	82	14	59	66	44
4	70	57	43	15	47	58	40
5	73	62	43	16	60	111	66
6	56	89	62	17	50	57	34
7	56	74	48	18	56,5	53	36
8	46	60	36	19	57	58	38
9	74	93	58	20	59,5	67	42
10	77	82	50	21	61	106	63
11	52,5	71	49	23	58,5	49	32
12	81	78	51	27	58	70	48
				28	67	123	62

The authors conclude that the agreement of the calculations from the radar and wavegraph observations suggests the existence of a coherent reflection of pulsed r-f signals from a wavy sea surface.

Kireyev, I. V., and A. V. Svechnikov. Results from studying radio wave reflection from a wavy sea surface. IN: Sb. Nekontaktnyye metody izmereniya okeanograficheskikh parametrov. Moskva, Gidrometeoizdat, 1975, 24-33. (RZhGeofiz, 9/75, #9V35). (Translation)

A model is considered for modulation of the envelope of a radar signal by orbital particle motion in the sea surface. On the basis of this model, the dependence of phase change in the envelope on para-

meters of wind waves is obtained. From the estimate of the contribution of wind waves to the signal, the authors conclude that the effect of wave heights is dominant. It is hence proposed to use the frequency of the envelope of a reflected signal for determination of wave heights. The results of related experiments are also given.

Lande, B. Sh., I. I. Mogretskaya, and N. P. Krasyuk. Spectral width of a uhf signal scattered by the sea surface, taking into account the air turbulence. IN: Sb. Prikladnyye zadachi rasseyaniya i difraktsii radiolokatsionnykh signalov. Leningrad, 1974, 16-19. (RZhF, 3/75, #3Zh131). (Translation)

The combined effect of sea waves and air turbulence on the spectral width of a scattered signal, generated by radiation from a high-resolution radar, is considered. It is shown that when air turbulence is accounted for, the spectral width of the reflected signal increases relative to the spectrum in a clear [calm] atmosphere.

Prakhov, V. P. On the effect of directivity pattern width of an antenna on the parameters of slope spectra, determined from reflected signal characteristics. IN: Nekontaktnyye metody izmereniya okeanograficheskikh parametrov. Moskva, Gidrometeoizdat, 1975, 104-110. (RZhGeofiz, 9/75, #9V45). (Translation)

From measurements of (averaged) slopes of a wavy surface, made under conditions of a finite radiation area, the slope spectra are found to differ from instantaneous slopes and their spectra. The relationship

between the spectra of average and instantaneous slopes is obtained on the basis of linear spectral theory for the Krylov frequency spectrum, multiplied by the angular distribution of energy $\cos^2\theta$. Similarly to a previously reached conclusion (Matushevskiy, 1969) in the case of measurements by a three-component coordinate indicator, the author shows that during measurements of slopes by radar, the diameter of the radiation area need not exceed 1/15 of the mean measured wavelength. The relationship developed enables one to determine the height of the radar antenna position, for a given directional pattern width, and vice versa.

Rayzer, V. Yu., Ye. A. Sharkov, and V. S. Etkin. Effect of temperature and salinity on radioemission from a smooth ocean surface in decimeter and meter ranges. FAiO, no. 6, 1975, 652-655.

The brightness temperature of the natural radiation of the ocean is calculated from:

$$T_{\vartheta}(\theta, \lambda) = \varkappa(\theta, \lambda)\, T_0 + [1 - \varkappa(\theta, \lambda)]\, T_H(\theta, \lambda), \tag{1}$$

where $\varkappa(\theta, \lambda)$ is the radiation of a smooth ocean surface which is in turn determined by the Fresnel coefficient $\dot{R}$, from the formula $\varkappa(\theta, \lambda) = 1 - \left|\dot{R}(\theta, \lambda)\right|^2$; T_0 is the thermodynamic temperature of the ocean; and $T_H(\theta, \lambda)$ is the radiobrightness temperature of the sky.

The complex dielectric permeability of the sea water is calculated from:

$$\dot{\varepsilon} = \varepsilon' - i\varepsilon'' = \frac{\varepsilon_s - \varepsilon_\infty}{1 + i(\lambda_s/\lambda)} + \varepsilon_\infty - i60\sigma\lambda, \tag{2}$$

where σ is the specific electrical conductivity, ϵ_s is the low frequency dielectric permeability, ϵ_∞ is the high frequency dielectric permeability, and λ_s is the critical wavelength, related to relaxation time by $\lambda_s = 2\pi c\tau$

The temperature and salinity dependence of ϵ_s, ϵ_∞, and λ_s are taken from the work of Hasted (1961), values of σ from Horn (1972). The results of the calculations are given in Figs. 1-4.

The work shows a definite correlation of radio emission from a smooth sea surface with temperture and salinity, for wavelengths in the decimeter and meter ranges.

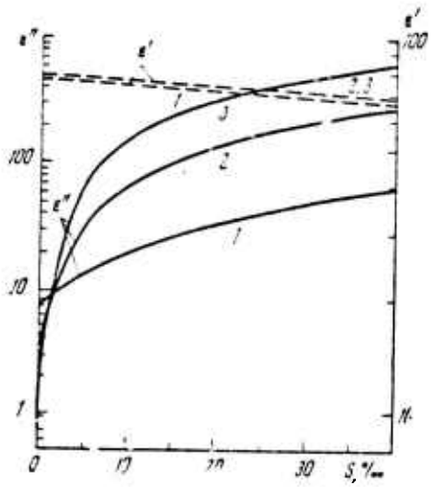

Fig. 1. Real ϵ' and imaginary ϵ'' parts of the complex dielectric permeability of sea water vs. salinity S, for wavelengths of 18 (1), 75 (2), and 200 cm (3) at $T = 20^{\circ}C$.

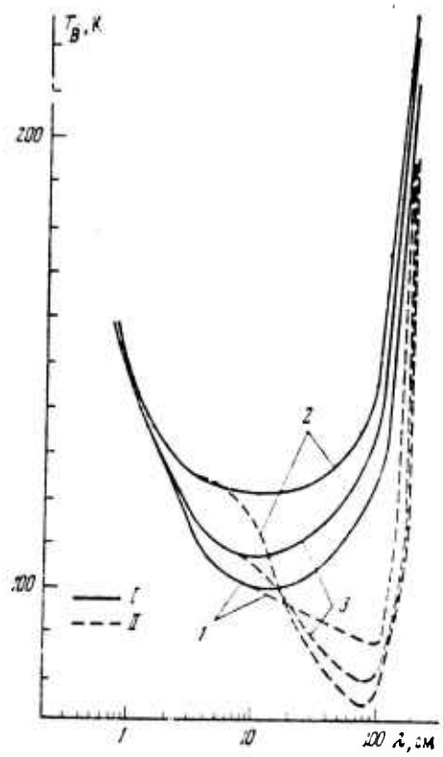

Fig. 2. Radiobrightness temperature T_B of sea surface vs. emission wavelength, from vertical observation at water temperatures of t = 0° C (1), 20° C (2), and 40° C (3) at S = 0‰(I) and 40‰(II).

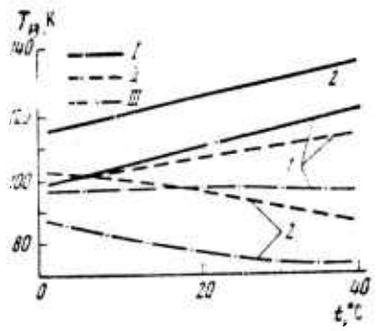

Fig. 3. Radiobrightness temperature T_B vs. water temperature t, from vertical observations for wavelengths of 18 (1) and 75 (2) cm at S = 0‰(I), 20‰(II), and 40‰(III).

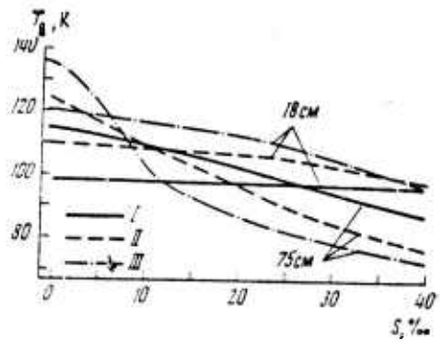

Fig. 4. Radiobrightness temperature T_B vs. salinity, for vertical observations at 18 (1) and 25 cm (2), at T = 0°C (I), 20°C (II), and 40°C (III).

Zamarayev, B. D., A. I. Kalmykov, I. V. Kireyev, A. S. Kurekin, V. Yu. Levantovskiy, V. V. Pustovoytenko, and A. V. Svechnikov. Methods of radar determination of wave characteristics. IN: Sb. Nekontaktnyye metody izmereniya okeanograficheskikh parametrov. Moskva, Gidrometeoizdat, 1975, 7-16. (RZhGeofiz, 9/75, #9V48). (Translation)

Physical principles are considered of a method for determining the parameters of wind waves, from signals reflected from a wavy sea surface. The possible use of incoherent centimeter-band radar is discussed. Results from measuring the intensity of reflected signals for various polarizations of transmitted and reflected signal are given. The spectrum of intensity fluctuations is proportional to the wave spectrum.

Zhilko, Ye. O., and A. A. Zagorodnikov. Radar stereo imaging of sea waves. IN: Sb. Nekontaktnyye metody izmereniya okeanograficheskikh parametrov. Moskva, Gidrometeoizdat, 1975, 42-50. (RZhGeofiz, 9/75, #9V37). (Translation)

A radar imaging method is considered which is analogous to a method for determining two-dimensional spectra of sea waves, from cross-sections along different directions of three-dimensional aerial wave photographs. Expressions are obtained for calculation of spectra using measured radar cross-sections. The basic difference between the two methods is that in the radar method, the slope of a wave surface is measured rather than its ordinate.

Zhilko, Ye. O., and A. A. Zagorodnikov. Measuring the group structure of sea waves by radar wavegraphs. IN: Sb. Nekontaktnyye metody izmereniya okeanograficheskikh parametrov. Moskva. Gidrometeoizdat, 1975, 51-54. (RZhGeofiz, 9/75, #9V38). (Translation)

By strobing a radar range gate along a given profile of a wavy surface, it is possible to obtain a nearly "frozen" profile and hence to determine the group structure of the waves. Measurements based on groups of 7-10 waves are given.

Belousov, P. S., A. A. Zagorodnikov, V. I. Korniyenko, and A. K. Kuklin. Results from experimental studies of measuring sea wave parameters by optical methods. IN: Sb. Nekontaktnyye metody izmereniya okeanograficheskikh parametrov. Moskva, Gidrometeoizdat, 1975, 146-152. (RZhGeofiz, 9/75, #9V47).

Wave flume experiments at the Ukrainian Academy's Marine Hydrophysical Institute, together with analysis of photographs, confirm that brightness of a wavy water surface is proportional to the derivative of its profile, and depends on the sign of the latter. The wide frequency range of the optical method enables one to apply the method in the study of the entire spectrum of sea wave slopes. An example is given of estimating the spectrum of small ripples using the optical method.

Martynova, Ye. A., and V. A. Spitsyn. Quantitative estimates of thermal radiation of an underlying surface using a scanning infrared apparatus. Trudy Arkticheskogo i Antarkticheskogo NII, no. 324, 1974, 197-203. (RZhGeofiz, 5/75, #5V34). (Abstract)

Methods are analyzed for estimating the temperature of surface objects by means of a thermal infrared scanner, as used for thermal mapping of snow and ice covers. Incorporating an IR-to-video converter enables one in principle to measure the temperature of objects studied. Simultaneous recording of temperature of an underlying surface and its thermal map can be realized by introducing a special standard source (absolute black body) against which the radiation of the test object is compared. Calibration of the IR system and characteristics of its receiving system are considered in detail.

Muro, E. L., and G. V. Pavlova. Determination of sea wave height and period from characteristics of optical signals reflected from the sea surface. IN: Sb. Nekontaktnyye metody izmereniya okeanograficheskikh parametrov. Moskva, Gidrometeoizdat, 1975, 133-141. (RZhGeofiz, 9/75, #9V46). (Translation)

The theoretical dependence is obtained of the relative intensity T_o of an optical signal, reflected by a disturbed sea surface, on the density of the reflecting area and overall curvature of the surface. Numerical calculations are made for the case of an isotropically disturbed sea surface, using Weyman's approximation for the frequency spectrum. Dependences of T_o on wind velocity, rms slope, and wave height are thus obtained. The article gives experimental data as well. The authors suggest determining mean wave period from the peak frequency of the spectrum of the reflected signal; this frequency approximately coincides with the peak frequency of the wind wave spectrum.

Polovinko, V. V. On optical sounding of the sea. IN: Sb. Nekontaktnyye metody izmereniya okeanograficheskikh parametrov. Moskva, Gidrometeoizdat, 1975, 153-157. (RZhGeofiz, 9/75, #9V56). (Translation)

Measurements of radiation of the sea surface were carried out in the Caspian Sea in the Neftyanyye Kamni region. They were accompanied by measurements of wave heights using a wire wave gage. A similarity between energy spectra of surface radiation and wave motion was observed.

Glotov, A. A., D. T. Matveyev, V. G. Mirovskiy, M. D. Rayev, I. A. Troitskiy, and V. S. Etkin. <u>Effect of waves on r-f thermal emission from a water surface.</u> Meteorologiya i gidrologiya, no. 8, 1975, 46-50.

Results are described of laboratory tests using a high-sensitivity centimeter-band radiometer (λ = 2.08 cm, δT = 0.03° C, τ = 1 sec) to measure radiative characteristics of small-scale roughness of a water surface. The experiment included wavegraph measurements of wave heights, h (see Fig. 1) The results are compared to theoretical calculations made by the method of small disturbances. A brief description of the experiment is included.

The increment in brightness temperature of the rough water surface is calculated by

$$|\dot{R}_B^{\cdot}(\Theta)|^2 = |\dot{R}_B(\Theta)|^2 (1 - 4 k^2 \sigma_h^2 \cos\Theta), \qquad (1)$$

where $\dot{R}(\theta)$ = Fresnel reflection coefficient for a smooth water surface in the case of vertical polarization; T = water surface temperature.

Constant β is determined during calibration of the antenna by a mirror + black body method. Variance for fluctuations of wave heights, σ_h^2, is calculated from measured wave spectra. Calculations of $T_B(\theta)$ are given in Fig. 2; these agree well with theoretical data. A block diagram of the radiometer is included.

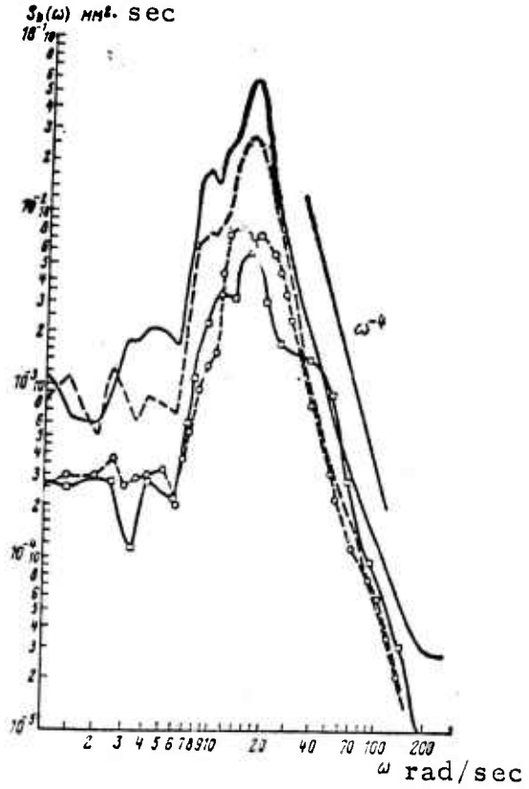

Fig. 1. Frequency spectra for waves in experimental tank (large-scale waves are not suppressed).

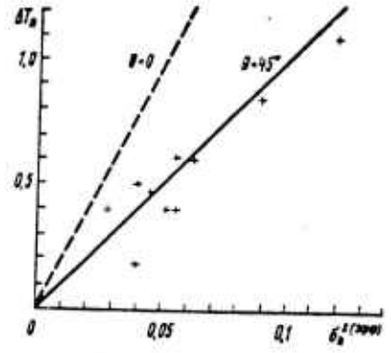

Fig. 2. Dependence of the increment of brightness temperature on σ_h^2.

Pereslegin, S. V. Statistical characteristics of superhigh-frequency scattering from the ocean surface allowing for finite resolution and for the depolarization factor. FAiO, no. 6, 1975, 610-619.

Mean intensity $\bar{\sigma}_\theta^2$ and spatial and temporal intervals r_θ and τ_θ in fluctuations of slopes of a sea surface as observed by a finite-resolution radar are calculated. The calculations are based on an analysis of r-f backscatter from the sea surface, which was made using an improved model of the isotropic spatial spectrum of sea surface relief which includes gravity and capillary intervals for small-scale waves. Using the concept of specific effective scattering area S_θ^o and an angular pattern of scattering, the author determines S_θ^o for large-scale and small-scale waves, as well as the wind increment in the zone of small-scale waves due to a random angle modulation by large-scale waves.

The calculations show that observations of a sea surface by a finite-resolution radar leads to decrease in the intensity of fluctuations for large-scale waves, as compared to point intensity, σ_θ^2. A decrease in intensity by a factor of 2 to 3 is observed when the diameter of the radiated area, r, is of the same order of magnitude as the effective spatial interval of fluctuations, $r_\theta \approx w_w^2/2g$; dependence on e-m wavelength disappears when $r \gg \lambda$. With $r > 2r_\theta$, intensity of fluctuations drops rapidly, especially for weak waves.

Averaging over space leads to an increase in the time interval of fluctuations, as compared to their point value ($\tilde{\tau}_\theta > \tau_\theta$); when $r > 2r_\theta$ the time interval for intense waves is less than the one for weak waves. Statistical characteristics of radio emission scattering area are identical to those of slopes of sea surface, but only for the vertically polarized component, which is characterized by small curvature of $S_{vv}^o(\theta)$. An exponential approximation of $S_{vv}^o(\theta)$ enables one to obtain simple analytical relations to mean value and variance of fluctuations of the specific effective scattering area.

3. Source Abbreviations

DAN SSSR	-	Akademiya nauk SSSR. Doklady
FAiO	-	Akademiya nauk SSSR. Izvestiya. Fizika atmosfery i okeana
RZhF	-	Referativnyy zhurnal. Fizika
RZhGeofiz	-	Referativnyy zhurnal. Geofizika
RZhMekh	-	Referativnyy zhurnal. Mekhanika
RZh. Vodnyy transport	-	Referativnyy zhurnal. Vodnyy transport
VMU	-	Vestnik Moskovskogo universiteta

4. Author Index to Abstracts